DISCLAIMER FOR FRONT PAGE OF MATERIALS TO BE MADE AVAILABLE VIA ETI INTERNET SITE

1. "Save to the extent set out in paragraph 2 below, this document and its contents are made available to you via the ETI's Internet Site "as is" without any representations, conditions, warranties or other assurance of any kind. The ETI and the authors, together with their employees, directors, servants or agents exclude to the maximum extent permissible by law all representations, warranties, conditions or other assurance whatsoever (whether express or implied) regarding the use of this document or its content including any warranties of title, merchantability, accuracy, completeness, non-infringement or that the document or its contents are of satisfactory or any particular quality or fit for any particular purpose. Any person accessing this document and using it or any of its contents accepts all risk in doing so.
2. Notwithstanding any statement to the contrary contained on the face of this document, the ETI confirms that the authors of the document have consented to its publication by the ETI."

Project	ReDAPT
Deliverable	MD1.5
Authors	I Afgan, DD Apsley, J McNaughton, S Rolfo, T Stallard, PK Stansby
Circulation	University of Manchester, EDF
To be approved by	Prof. Dominique Laurence
Date	27 June 2013
Version	0.5

CFD Simulation of Turbulence at a Tidal Stream Site based on Field Measurements

by

I Afgan, DD Apsley[1], J McNaughton, S Rolfo, T Stallard, PK Stansby
School of MACE
University of Manchester

[1] Corresponding Author

EXECUTIVE SUMMARY

This document represents deliverable MD1.5 and describes the application of EDF's open-source CFD solver *Code_Saturne* to a full tidal-stream turbine simulation, with realistic ambient flow conditions, as well as LES simulations to characterise the turbulence in a channel flow which will inform inflow conditions for the main LES calculations in MD1.4.

The two main achievements of this stage are:

- full RANS simulation of the 1MW TGL turbine at a fixed rotation rate, including effects of turbulence and mean-flow velocity shear with realistic ebb and flood profiles from the EMEC test site;
- high-resolution channel-flow calculations to characterise mean velocity, turbulence and length scales in fully-developed flow and assess the performance of synthetic eddy methods (SEM) for providing inflow conditions for future LES simulations of the TGL turbine.

The primary findings of the RANS simulations are:

- *whole-rotor* thrust and power coefficients are about 0.82 and 0.41 respectively, with only minor variations with turbulence intensity and inflow velocity shear ...
- ... but considerable variation in *individual blade* thrust and power coefficients (about 20% in thrust and 30% in power over a complete rotation) as a result of non-uniform mean velocity, with much smaller influence of mast and turbulence intensity;
- if applied at inlet then the 10% levels of turbulence typical of the EMEC test site would substantially diffuse the ebb and flood sheared profiles before they reached the turbine rotor.

The major findings of the LES channel-flow simulations are:

- Code_Saturne's fully-developed (periodic) LES simulations are in excellent agreement with independent DNS simulations at $Re_\tau = 150$ ($Re_b = 2300$), validating the approach used here.
- The wall-function approach successfully overlaps with fully-resolved wall treatment at $Re_\tau = 1020$ ($Re_b = 20000$), providing confidence in its application to higher Reynolds numbers. In general, wall-function profiles giving a smoother transition from linear sublayer to log layer gave results less sensitive to the size of the near-wall cell.
- At low Reynolds numbers the divergence-free synthetic-eddy model (DFSEM), with vorticity-carrying eddies, demonstrates faster approach to fully-developed flow than the original synthetic eddy model (SEM). However, difficulties with its implementation do not provide compelling evidence of its advantages over the older model at high Reynolds numbers. With the original SEM, the weakly correlated length scales have little effect on the flow development length.
- The meshes used for the present (RANS) turbine calculations are much coarser than that required for LES. Initial estimates are that the number of cells required to establish the effects of turbulence on the loading of the turbine (which is what is required of this project) will be in the order of 20-30 million cells. The possibility of hybrid LES/RANS simulations, (well-developed, implemented in *Code-Saturne* and validated by the University of Manchester over several airfoil-aerodynamics EU projects with EADS) might be considered in the future as a fully-resolved LES (both near-turbine and wake) would be computationally very expensive.

CONTENTS

1. INTRODUCTION
1.1 Scope of this document
1.2 Specific tasks associated with this project
1.3 ETI acceptance criteria for MD1.5
1.4 Staff on the project

2. RANS SIMULATION OF THE 1 MW TGL TURBINE
2.1 Overview
2.2 Representative inflow velocity profiles and the effect of turbulence
2.3 Description of the turbine simulation
2.4 Results

3. SIMULATIONS TO DETERMINE SUITABLE INLET CONDITIONS FOR LES
3.1 Computational model
3.2 Synthetic eddy models
3.3 Cases considered
3.4 Results for fully-developed flow
3.5 Results with synthetic-eddy methods for developing flow

4. OUTLINE OF FUTURE WORK
4.1 Computational mesh
4.2 Specification of turbulence and velocity profile
4.3 Specification of mechanical aspects

REFERENCES

1. INTRODUCTION

1.1 Scope of this Document

This report explains the work undertaken to complete milestone MD1.5; specifically:

- RANS simulations of the TGL 1 MW turbine at a prescribed rotation rate, including the effects of turbulence and realistic inflow velocity shear;
- LES calculations with both fully-developed (periodic[2]) and synthetic inflow turbulence to establish the appropriate inflow conditions for large-eddy simulation of the 1 MW turbine.

1.2 Specific Tasks Associated With This Project

The specific milestones for the CFD work on the ReDAPT project are as follows. Major items in this report are in bold.

MD1.1	Ideal turbine geometry. Imposed rotation of a single cylindrical mesh (Coriolis forces or ALE). RANS turbulence. No waves. Report to identify development necessary for sliding mesh.
MD1.2	Ideal turbine geometry. Rotation via sliding mesh (including a description of the method). RANS and LES turbulence. Presentation of formulation and assumption of model and first assessment of the influence of turbulence model and characteristics on transient loads.
MD1.3	TGL 1 MW turbine and structure geometry. Rotation imposed via new sliding-mesh method. RANS only simulation. Waves (modelled by ALE) and assessment of the influence of waves on transient loads and output.
MD1.5 (This Report)	**Establishment of representative mean-velocity profiles at a tidal stream site, based on field measurements. RANS simulations of the effect of shear profiles of velocity and (isotropic) turbulence on unsteady loading of 1 MW turbine. Structure of anisotropic turbulence established by LES simulations of undisturbed flow with SEM inflow turbulence. Summary of the inflow parameters required to represent EMEC flow in the LES simulations of MD1.4.**
MD1.4 (Delayed by absence of data; due 2014)	LES simulations with the TGL 1 MW turbine and structure geometry. Rotation imposed via sliding mesh method. Assessment of the effects of turbulence and waves on transient loads and power output.

[2] "periodic" means that the outflow is reintroduced as the inflow many times, thus representing an "infinite channel" of constant cross section driven by space-time-constant pressure gradient.

1.3 ETI Acceptance Criteria For MD1.5

The specific ETI Acceptance Criteria for MD1.5 are the following.

A. Structure of isotropic turbulence at tidal site based on field measurements of velocity depth profile (RANS simulation of flow only).

B. Effect of shear profiles of velocity and corresponding turbulence on unsteady loading of 1 MW tidal stream turbine (RANS simulation of flow and rotor);

C. Structure of anisotropic turbulence at tidal stream site based on field measurements of velocity depth profile (LES simulation of flow only, with synthetic eddy model of turbulence).

D. Summary of the turbulence inflow parameters required to represent flow at the EMEC site in the LES simulations of unsteady rotor loading that will be conducted for MD1.4.

Items A and B are to be found in Section 2 of this Report and are part of a bigger investigation that has been published as the PhD thesis of James McNaughton.

The objective of part C, which is reported in Section 3 of this report, is to determine an appropriate method for representing the incident flow as measured at the EMEC deployment site in a Large Eddy Simulation. This is required to define the inflow to the LES simulations of turbine loading that will be conducted in MD1.4.

1.3.1 Inflow Data Needed for LES

The inflow across a vertical plane upstream of the turbine is defined in terms of the depth profile of mean velocity and, depending on the CFD turbulence model employed, of some characteristics of the flow turbulence. For input to LES it is necessary to define a time series of velocity fluctuations at each mesh point, such that specified statistical properties of the turbulence are reproduced. Various methods are available for producing a velocity field with specified turbulence properties (see Section 3). In MD1.2 an existing Synthetic Eddy Method (SEM) was employed with a uniform depth profile of mean velocity to compare LES simulations to RANS simulations. A drawback to the standard SEM method is that a relatively long distance is required before the turbulence statistics are fully developed. An alternative Divergence-Free Synthetic-Eddy Method (DFSEM) is now available, which it was hoped would allow turbulence to develop over a shorter distance. These approaches are evaluated.

1.3.2 Inflow Data Available

An objective of MD3 is to obtain high-resolution measurements of the spatial variation of the EMEC flow in the vicinity of the turbine. The desirable and feasible set of flow parameters to be measured is identified in MD3.4. In summary the desirable dataset is a depth profile of mean velocity, Reynolds stresses and integral length scales. The instrumentation developed in MD3 is expected to provide mean-velocity depth profile, principal components of Reynolds stresses at mid-depth and principal length-scales at mid-depth. The CFD studies conducted provide some insight into which parameters are of particular importance for defining the CFD inflow to represent the measured flow.

1.3.3 Outline of MD1.4 Simulation (Due March 2014)

The mesh resolution required for an LES simulation of channel flow is dependent on the Reynolds number Re_τ (= $u_\tau h/\nu$ – see later). The EMEC flow has a depth of approximately 40 m and flow speeds up to 3 m s^{-1} are of interest. This corresponds to a bulk Reynolds number of approximately 6×10^8 or Re_τ approximately 630000. A prohibitively large cell count would be required to resolve the channel bed at this Reynolds number, so a wall-function approach will be employed at the bed. The mesh will be resolved to the geometry of the blades.

1.3.4 LES Channel-Flow Investigations

To develop an appropriate method of defining a turbulent inflow to the LES simulation the following have been investigated and are reported in Section 3.

- Assessment of mesh dependency of LES of channel flow.
- Selection of wall-function and assessment of influence on turbulence.
- Selection of appropriate Synthetic Eddy Method and inflow parameters.
- Assessment of the development of mean profile and modelled turbulence .

1.4 Staff on the Project

The research staff employed on this project are a PhD student (James McNaughton) and a post-doctoral research associate (Dr Stefano Rolfo). The academic staff associated with the project are Prof. Peter Stansby, Dr Imran Afgan, Dr David Apsley and Dr Tim Stallard.

2. RANS SIMULATIONS OF THE 1MW TGL TURBINE

2.1 Overview

This Section summarises the main findings of the RANS simulations performed for the 1 MW TGL turbine. A comprehensive description of the test case can be found in the PhD Thesis of James McNaughton (to be made publicly available by the University of Manchester after his viva). The results presented in this section are also due to be presented at the European Wave and Tidal Energy Conference 2013. The conference paper, which includes more technical details as well as some discussion on the wake characteristics, is attached as an appendix to this work.

2.2 Representative Inflow Velocity Profiles and the Effect of Turbulence

To assess the effect of realistic flow conditions on the turbine's performance, the development of several inflow velocity profiles was considered. These were provided in ReDAPT report MA1001 PM14 MD5.2 and are shown in Figure 2.1 for the accelerating flood and decelerating ebb tides, with depth-averaged mean velocity of $U_0 = 1.8$ m s^{-1}.

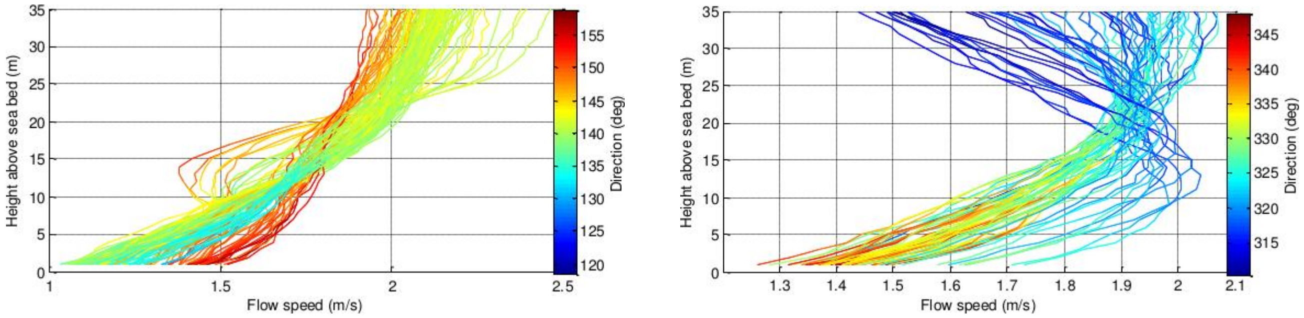

(a) Flood accelerating flow   (b) Ebb decelerating flow

Figure 2.1: ADP data for the Fall of Warness test site.

One velocity profile from each of these conditions was selected for assessment. In addition, a uniform velocity profile was used as a baseline. The three characteristic profiles used in this Report are shown in Figure 2.2 and referred to as Uniform, Flood and Ebb velocity profiles.

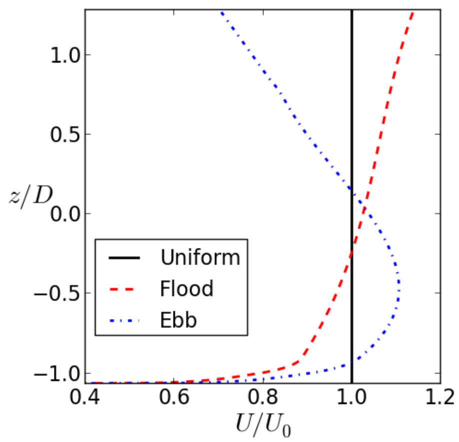

Figure 2.2: Velocity profiles used in the present study.

Measured profiles of turbulence intensity (TI), *I*, are not available from the test site, but are expected to be about 10%. One initial objective was to find TI profiles that would maintain the shape of each mean-velocity profile from the inlet to the turbine rotor plane. However, two-dimensional channel calculations conducted to establish the evolution of each profile demonstrated that such high TI caused the shape of the Flood and Ebb velocity profiles to change significantly. Figure 2.3 shows the developed mean-velocity profile when uniform inflow turbulence levels of 1% and 10% were considered. From these computations it was concluded that to maintain the shape of the Flood and Ebb velocity profiles, only very low turbulence levels could be specified at inlet. Thus, the effect of inflow turbulence levels in the following sections was only considered for a uniform inflow velocity.

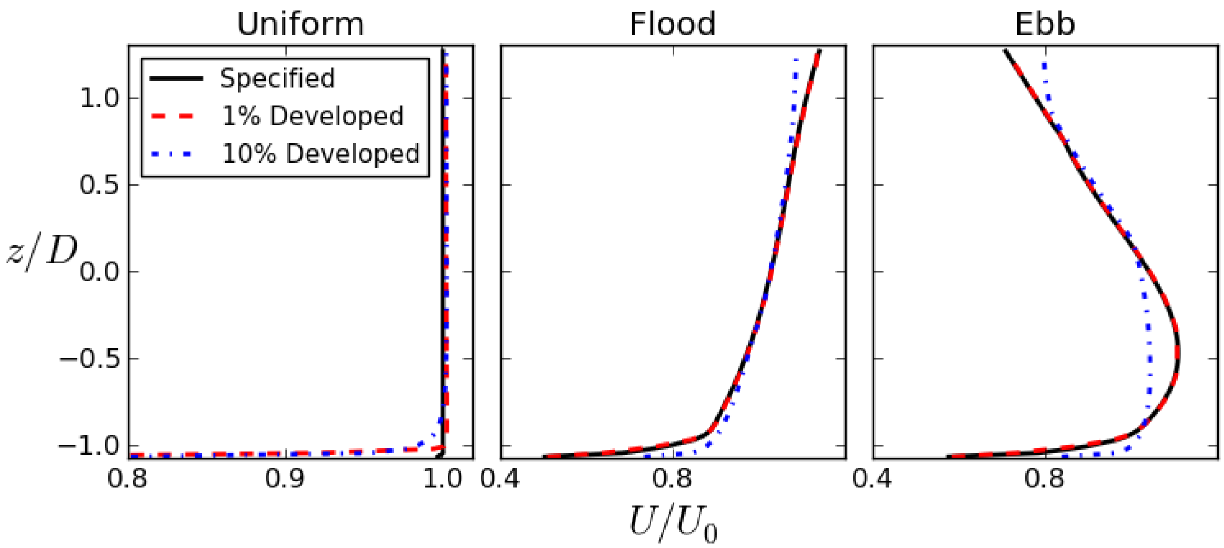

Figure 2.3: Effect of inlet turbulence intensity on each of the velocity profiles.

2.3 Description of the Turbine Simulation

The geometry and meshing strategy were described in ReDAPT report MA1001 MD1.3 and so are only briefly discussed here. A block-structured approach was used to maximise control of the cell distribution and total number of cells, whilst also permitting a high-quality mesh around the blades. The surface mesh is shown in Figure 2.4a with the complete domain shown in Figure 2.4b. 106 cells were placed around the blade profile and 75 along its length, with refinement at both the leading and trailing edges, as well as towards the blade tip. In total 8.4 million cells were used, with a ratio of 2:1 between the outer and inner domains respectively. Whilst not the focus of the results presented in the current report, this allowed sufficient resolution to study the flow physics in the near wake as well as determining the loading coefficients.

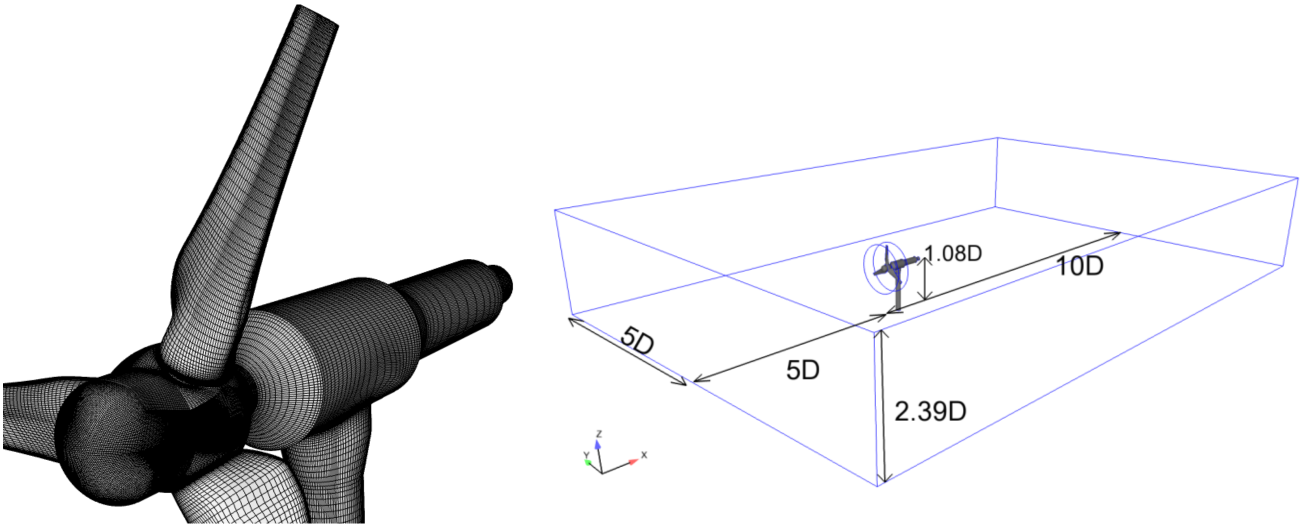

(a) View of the surface mesh (b) Dimensions of domain used.

Figure 2.4: Overview of geometry and mesh.

Following an assessment of different RANS models (McNaughton et al., 2012) the k-ω turbulence model was chosen. The turbulent kinetic energy, k, and specific dissipation rate, ω, required at the inlet were specified in terms of the local mean velocity by

$$k = \tfrac{3}{2} I^2 U^2, \qquad \omega = \frac{k^{1/2}}{C_\mu^{1/4} L}$$

with $C_\mu = 0.09$ and L a length scale taken as 0.7 times the turbine hub height following previous recommendations (Gant and Stallard, 2008).

In the following results the effects of velocity shear were examined by considering Ebb, Flood and Uniform mean-velocity profiles at a turbulence intensity of 1%, whilst the effects of inflow turbulence were examined by computing the flow with the Uniform mean-velocity profile only at a turbulence intensity of 10%.

2.4 Results

Results were obtained for each of the velocity profiles with a fixed angular velocity Ω, corresponding to a constant tip-speed ratio (TSR) of 6 (based on BEM simulations of TGL), where

$$TSR = \frac{\Omega R}{U_0}$$

where R is the blade radius and U_0 a suitable reference velocity (see below).

Due to the depth at the turbine deployment location (43 m) being deeper than that where the velocity profiles were obtained (35 m) the profiles are extrapolated over the extra depth. As a result the depth-averaged velocity was no longer 1.8 m s^{-1}. Several alternatives were considered for U_0:

- U_D depth-averaged velocity;
- U_A mean velocity over turbine swept area;
- U_H velocity at hub height.

The values of each of the above velocity scales for the three velocity profiles considered in this work are presented in Table 2.1. The values of U_A are approximately equal to U_H (because the fraction of the rotor area is greatest at its mid-height), but quite different from the depth-averaged velocity, U_D. U_A is the velocity scale that gives the most physical representation of available power; hence, it is the scale used in the following results.

Velocity	Uniform	Flood	Ebb
U_D	1.8	1.826	1.712
U_H	1.8	1.844	1.870
U_A	1.8	1.839	1.853

Table 2.1: Velocities (in m s^{-1}) used for normalisation.

As a result of the choice of velocity scale, the TSR and mean loading coefficients change, as shown in Table 2.2. Since we used a limited computational domain (albeit with a relatively low blockage ratio of 3.3%) blockage-corrected values are also shown in the table, using the blockage correction described in Bahaj et al. (2005).

	Raw values			Blockage-corrected values		
	TSR	C_T	C_P	TSR	C_T	C_P
Uniform (I = 1%)	6.00	0.845	0.431	5.91	0.819	0.411
Uniform (I = 10%)	6.00	0.862	0.430	5.90	0.834	0.409
Flood	5.87	0.845	0.435	5.78	0.819	0.415
Ebb	5.83	0.850	0.443	5.74	0.824	0.423

Table 2.2: Tip speed ratio, thrust and power coefficients using U_A as velocity scale.

The effect of an increased inflow turbulence has negligible effect on the power coefficient, but the thrust increases by about 2%. When normalised by U_A, approach-flow velocity shear has only marginal influence on thrust and power coefficients for the whole rotor.

For individual blades, however, the effect of velocity shear on loading coefficients during the course of a rotation is very pronounced. Figure 2.5 shows the instantaneous loading coefficients, phase-averaged over a rotation and normalised by their mean over a complete rotation. Here, the velocity scale in the denominator is irrelevant as it cancels through normalising with the mean.

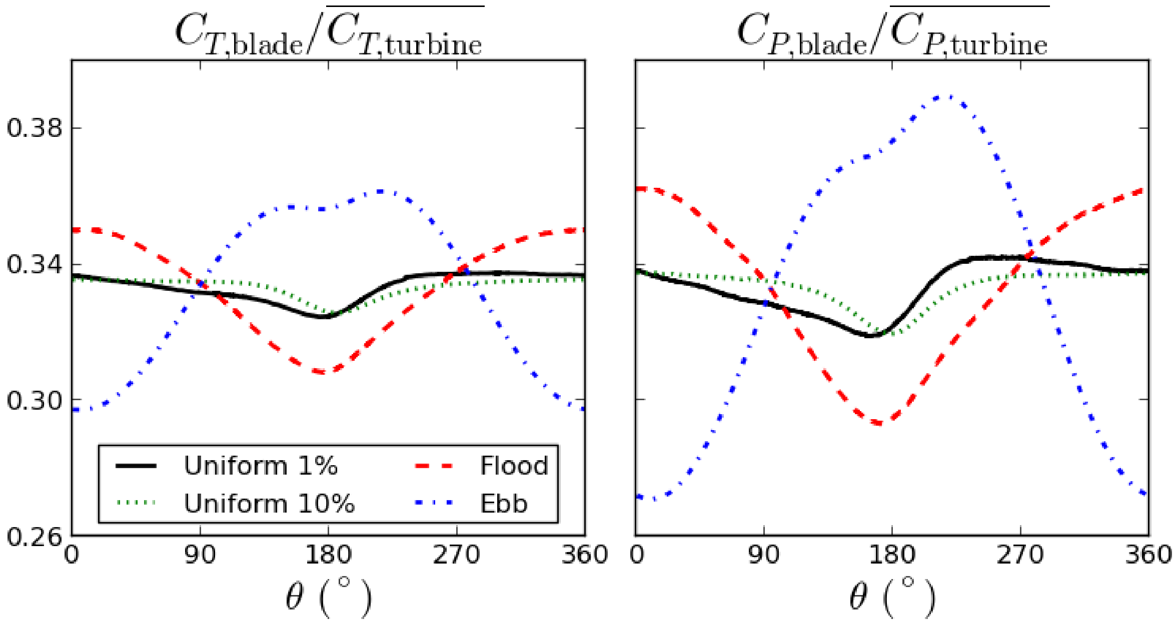

Figure 2.5: Phase-averaged thrust and power coefficients for each velocity profile.

For a uniform mean velocity inflow, several factors contribute to non-uniform load coefficients for a single blade; these include the mast and the non-permeable side and top/bottom boundaries. For the uniform-mean, 1% turbulence inflow minimum thrust and power coefficients occur near where the blade passes in front of the mast; at this point the pressure difference across the rotor is reduced by the increased downstream pressure. The power coefficient shows greater variation than the thrust. Minimum load coefficients do not occur at precisely 180º, where the blade is aligned with the mast, but slightly earlier, at 175º and 164º for thrust and power respectively. Similarly, maxima occur at 301º (thrust) and 257º (power). The overall variations in these coefficients, defined as $(\phi_{max} - \phi_{min})_{blade} / \phi_{av,turbine}$, are 1.3% and 2.3% for thrust and power coefficients respectively. When the inflow turbulence intensity is raised to 10% the variations in coefficients is slightly less (1% and 1.8% for thrust and power respectively), with maximum and minimum of each coefficient occurring slightly later in the rotation. As shown in Table 2.2 the overall thrust on the whole rotor increases slightly for the 10% TI case.

The effect of the sheared inflow-velocity profiles (which have only been computed with an inflow turbulence intensity of 1%) is much more significant than that due to increased turbulence intensity. Substantially greater variations are observed during the course of a rotation as a direct result of the depth-varying velocity, with the greatest value of each coefficient related to the maximum velocity (in the upper part of the channel, near 0º, for the Flood profile; in the lower part of the channel, near 180º, for the Ebb profile). The variations in power coefficients over a cycle are 6.4% and 11.9% for Flood and Ebb profiles respectively. The mast effect is not evident for the Flood profile because the approach-flow velocity is low at this point in the cycle region, but is visible for the Ebb profile.

Finally, as it is intended to make a comparison with the corresponding experimental data that will be available in MD1.4, flap and edgewise bending moments are calculated at the blade root ($r/R = 0.27$) and an intermediate position ($r/R = 0.44$), in accordance with the position of strain gauges on the 1MW TST. These are defined in Figure 2.6. Flapwise moments are taken about the chord-line whereas edgewise moments are taken about a line that is perpendicular to 35% of the chord line.

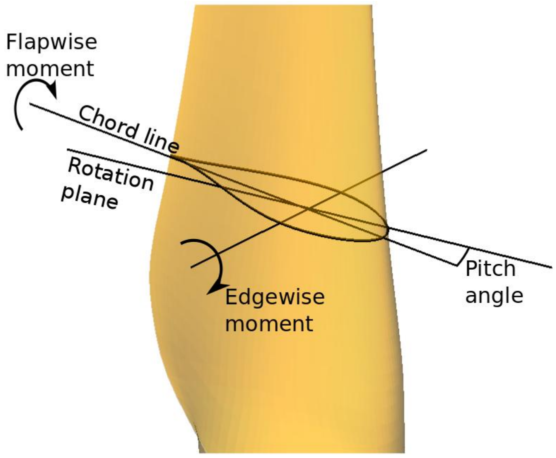

Figure 2.6: Definition of axis for flapwise and edgewise moments.

Phase-averaged bending moments over a rotation for each inlet velocity profile are shown in Figure 2.7, where the moments have been non-dimensionalised as the following coefficient:

$$C_M = \frac{M}{\frac{1}{2}\rho\pi R^3 U_0^2}$$

where M is the moment. From these plots it is clear that the increase of turbulence intensity has far greater effect on the edgewise moments and would contribute to a degradation in the turbine's performance. The mast effect is visible for the Uniform flow profiles, but is significantly less than the variations in root and mid-flapwise bending moments, which are 3.8 and 6.0 times greater for Flood and Ebb velocity profiles respectively.

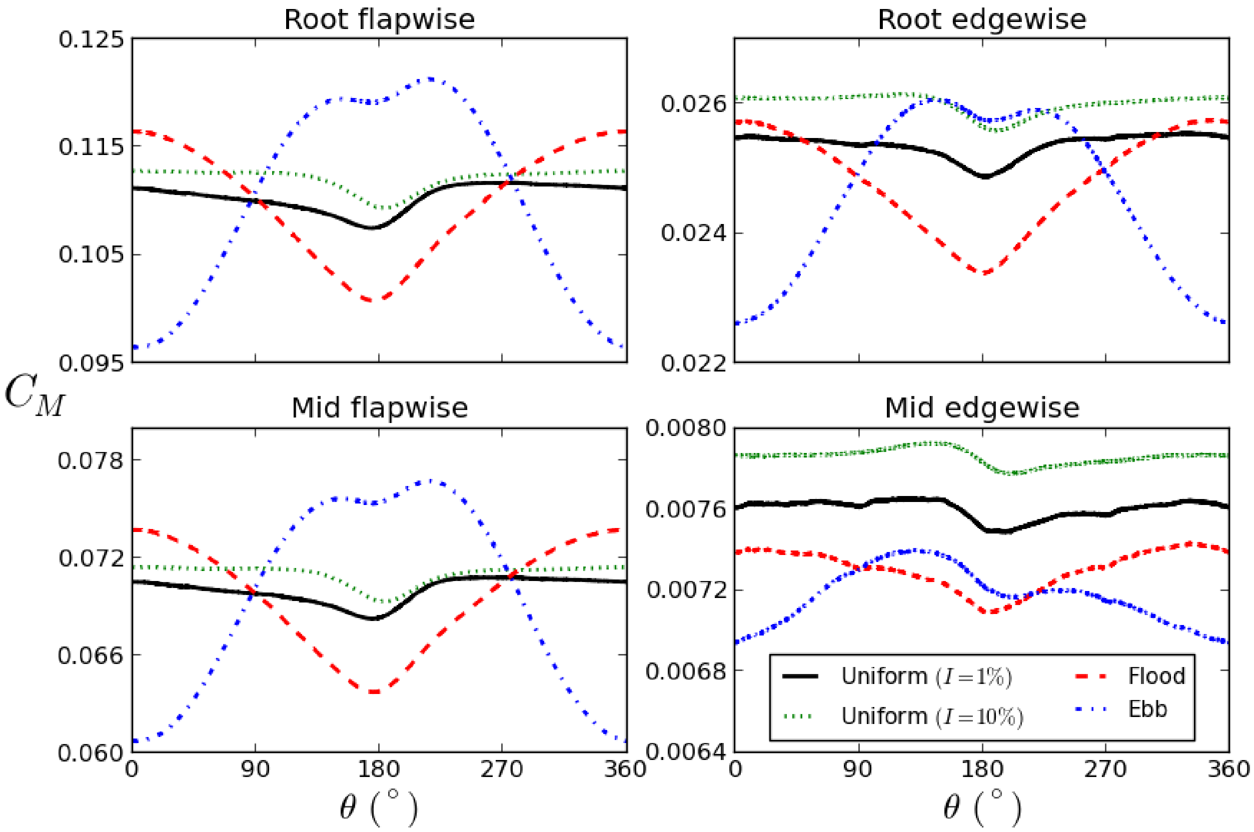

Figure 2.7: Phase-averaged bending-moment coefficients.

3. SIMULATIONS TO DETERMINE SUITABLE INLET CONDITIONS FOR LES

In the previous section RANS simulations were reported for the 1 MW TGL turbine in typical tidal-flow conditions. In the next phase of the project similar calculations will be conducted with LES modelling of turbulence. LES, however, requires much more information at inlet: in particular, a time-series of velocity fluctuations with suitable statistical properties of Reynolds stress and length scales.

A number of existing methodologies can be used to generate these time series. These include: imposing random fluctuations at the inlet; imposing space-correlated fluctuations; recycling the velocity profiles from a downstream plane; imposing spectral distributions of fluctuations using geometric functions, where the spectral signature is approximated by a modified von Kármán spectrum. Although these techniques work to some degree there is a considerable computational cost associated with the turbulence development. In many of these methods the imposed fluctuations are made up of components which are only weakly correlated. This causes the imposed turbulence to decay rapidly.

A way around these problems is to use a Synthetic Eddy Method (SEM). As a necessary precursor to the use of SEM and its variants, a series of well-resolved channel-flow simulations has been undertaken to establish appropriate boundary conditions for future LES calculations. In particular we have conducted:

- fully-developed simulations (with periodic boundary conditions) to establish typical mean and turbulent flow profiles and candidate length scales at a range of Reynolds numbers;
- developing-flow simulations to test inflow turbulence synthesisers – both standard model and newer divergence-free synthetic-eddy methods – to test their suitability for generating a fluctuating inlet velocity field.

3.1 Computational Model

3.1.1 LES Equations

The continuity and momentum equations for the filtered velocity components (u_i) are, in conservative form,

$$\frac{\partial u_j}{\partial x_j} = 0$$

$$\frac{\partial}{\partial t}(\rho u_i) + \frac{\partial}{\partial x_j}(\rho u_i u_j) = -\frac{\partial p}{\partial x_i} + \frac{\partial}{\partial x_j}\left[(\mu + \mu_{SGS})(\frac{\partial u_i}{\partial x_j} + \frac{\partial u_j}{\partial x_i})\right]$$

The Smagorinsky model is used for the subgrid-scale eddy viscosity:

$$\mu_{SGS} = \rho(C_s\Delta)^2 Sf$$

where

$$C_s = 0.065$$

$$\Delta = 2(cell\ volume)^{1/3}$$

$$S = \sqrt{2S_{ij}S_{ij}}\ , \qquad \text{where } S_{ij} = \frac{1}{2}\left(\frac{\partial u_i}{\partial x_j} + \frac{\partial u_i}{\partial x_j}\right)$$

and the Van Driest low-Re damping function is

$$f = 1 - e^{-y^+/26}$$

3.1.2 Boundary Conditions

Streamwise and lateral boundaries

For fully-developed boundary-layer simulations periodic boundary conditions were applied in both streamwise (x) and spanwise (z) directions. For developing boundary-layer simulations SEM (with two choices of length scales) and DFSEM were employed to specify inlet boundary conditions.

The entire pressure itself cannot be treated as periodic because there must be a streamwise pressure gradient to balance the (prescribed) frictional drag on the bottom wall. Balancing average forces for the whole domain (depth h and length L):

$$(p_1 - p_2)h = \tau_w L$$

whence

$$\frac{p_1 - p_2}{L} = \frac{\tau_w}{h}$$

This is incorporated as a body force per unit volume of:

$$-\frac{\mathrm{d}\bar{p}}{\mathrm{d}x} = \frac{\rho u_\tau^2}{h}$$

with the code then solving for the additional pressure fluctuations.

Top Boundary ($y = h$)

Given the low Froude number of the intended calculations this was treated as a stress-free rigid lid:

$$v = 0, \qquad \frac{\partial u}{\partial y} = \frac{\partial w}{\partial y} = 0, \qquad \frac{\partial p}{\partial y} = 0 \qquad \text{on } y = h.$$

Lower Boundary ($y = 0$)

This is treated as either:
(i) fully-resolved, using viscous damping in the sub-grid-scale (SGS) eddy-viscosity model;
(ii) using wall functions.

In the first case the near-wall node is placed well within the laminar sublayer. In the second case the near-wall node is within the log layer and one of two theoretical profiles is assumed for the unresolved near-wall behaviour:

Standard *Code_Saturne* approach:

$$u^+ = \begin{cases} y^+ & \text{if } y^+ \le 10.88 \\ \dfrac{1}{\kappa}\ln y^+ + 5.2 & \text{if } y^+ \ge 10.88 \end{cases}$$

The composite wall law of Reichardt (1951):

$$u^+ = \frac{1}{\kappa}\ln(1 + \kappa y^+) + 7.8(1 - e^{-y^+/11} - \frac{y^+}{11}e^{-y^+/3})$$

In both cases the wall-unit definitions are

$$u^+ = \frac{u}{u_\tau}, \qquad y^+ = \frac{u_\tau y}{\nu}$$

and these are used to determine the local friction velocity u_τ (and hence the wall shear stress) from the near-wall values of tangential velocity u and wall-normal distance y.

3.2 Synthetic Eddy Models

The objective of synthetic eddy modelling is to supply an LES calculation with a fluctuating inlet velocity field with the intended statistical distribution of Reynolds stresses and turbulent length scales. The synthetic eddy models available in Code_Saturne (or implemented for the present work) are:

- two variants of the original SEM model(s) based on the work of Jarrin et al., 2006, 2009;
- the divergence-free synthetic-eddy model (DFSEM) of Poletto, 2011.

In both types of model fluctuating velocities are generated from eddies advected through a virtual box (volume V_B) containing the nominal inlet plane. As each eddy leaves the box another eddy is regenerated at a random location on the box inlet plane.

3.2.1 Original SEM (Jarrin et al., 2006, 2009)

$$u_i'(\mathbf{x}) = \frac{1}{\sqrt{N}} \sum_{e=1}^{N} a_{ij} \varepsilon_j^e f_L(\mathbf{r}^e) \qquad \text{(Equation 3.1)}$$

where

$\mathbf{r}^e = \mathbf{x} - \mathbf{x}_e$ is the displacement relative to the centre $\mathbf{x}_e$ of eddy e

N is the number of eddies in the box

a_{ij} are the Lund coefficients (Cholesky decomposition of $\overline{u_i u_j}$)

ε_j^e are a set of random numbers with mean 0 and variance 1 for eddy e

$f_L(\mathbf{x}) = \sqrt{\frac{V_B}{L^3}} f(\frac{x}{L_x}) f(\frac{y}{L_y}) f(\frac{z}{L_z})$

L_x, L_y and L_z are length scales (see below), with $L = \frac{1}{3}(L_x + L_y + L_z)$

f is a shape function; typically the triangular function $f(\xi) = \max(\sqrt{\tfrac{3}{2}}(1 - |\xi|), 0)$

3.2.2 Divergence-Free SEM (Poletto et al., 2011)

The motivation for this was to reduce the required flow-development length and large pressure fluctuations at inlet observed with the original SEM by imposing a divergence-free condition on the eddy field. This is naturally achieved by basing it on the *vorticity* carried by the eddies.

The initial DFSEM used a single length scale L, as in the SEM model. However, this lacked the flexibility to represent high turbulence anisotropy. In the present form there may be length scales L_1, L_2, L_3 along each of the principal axes of the Reynolds stress tensor. The eddy field is first deduced along principal axes (along which the Reynolds stress tensor is diagonal):

$$u_\alpha'(\mathbf{x}) = \frac{1}{\sqrt{N}} \sum_{e=1}^{N} q_\alpha (\mathbf{r}^e \wedge \boldsymbol{\alpha}^e) \qquad \text{(Equation 3.2)}$$

and then rotated to the global axes. Here, α are vectors setting the "intensity" of the eddy along each axis. The shape function q_α has the form

$$q_\alpha = L_\alpha \left[1 - (\frac{r_\alpha}{L_\alpha})^2 \right]$$

3.2.3 Length Scales

These appear in the shape functions. It is to be expected that the length (and time) scales imposed at inlet have a considerable influence on the development length of the turbulence. In the original SEM it is possible to use a single isotropic length scale

$$L = \frac{k^{3/2}}{\varepsilon}$$

(where k is the turbulent kinetic energy and the dissipation rate ε is estimated as $2\nu\overline{S}_{ij}\overline{S}_{ij}$).

An appropriate extension that permits normal-stress anisotropy is

$$L_{\alpha\alpha} = \frac{(\frac{3}{2}\overline{u_\alpha^2})^{3/2}}{\varepsilon}$$

Alternatively, a more advanced treatment based on two-point correlations leads to integral length scales

$$L_{\alpha\alpha}(\mathbf{e}) = \frac{1}{R_{\alpha\alpha}(0)}\int_0^\infty R_{\alpha\alpha}(r\mathbf{e})\ \ \mathrm{d}r$$

where

$$R_{\alpha\alpha}(\mathbf{r}) = < u_\alpha(\mathbf{x},t)u_\alpha(\mathbf{x}+\mathbf{r},t) >$$

and both streamwise and spanwise correlations (i.e. the direction of unit vector **e**) may be considered.

3.2.4 Variants of Synthetic-Eddy Model

Three synthetic-eddy methods were considered during this study.

- SEM_Saturne
  This is coded by default in *Code_Saturne* (v3) and uses 3 stress-based length scales; i.e. each velocity component uses $L_x = L_{11}$, $L_y = L_{22}$, $L_z = L_{33}$.

- SEM_Jarrin
  This uses integral length scales in the relevant velocity-component directions if homogeneous (i.e x and z) and a length scale based on the vertical stress if not (y): a total of 7 length scales.
  - u': use $L_x = L_{11}(x)$, $L_y = L_{22}(x)$, $L_z = L_{33}(x)$, streamwise integral length scales
  - v': use $L_x = L_y = L_z = L_{22}$, based on the wall-normal stress velocity fluctuations
  - w': use $L_x = L_{11}(z)$, $L_y = L_{22}(z)$, $L_z = L_{33}(z)$, spanwise integral length scales

- DFSEM
  The divergence-free synthetic-eddy model. Effectively this uses 3 length scales, based on a single base length scale and specified ratios of length scales along the principal axes.

3.3 Cases Considered

All calculations have been computed in non-dimensional form, using friction velocity u_τ and depth h as the velocity and length scales respectively. (Non-dimensional forms of the incompressible flow equations can be obtained by setting ρ = 1 and replacing the molecular viscosity μ by $1/\mathrm{Re}_\tau$). Here,

$$\mathrm{Re}_\tau = \frac{u_\tau h}{\nu}$$

To compare with the more-easily-measured bulk Reynolds number:

$$\mathrm{Re}_b = \frac{U_b h}{\nu},$$

where U_b is the bulk velocity, fixed by the flow rate, we have used the following empirical correlation due to Pope (2000) in the following table:

$$\mathrm{Re}_b = \frac{1}{2}\left(\frac{\mathrm{Re}_\tau}{0.09}\right)^{1/0.88}$$

Calculations are either:

- fully-developed shear flow, using periodic streamwise (x) and spanwise (z) boundary conditions; or
- developing flow, using SEM or DFSEM to impose synthetic turbulence on top of the mean velocity profile from the fully-developed case.

In the following table, the mesh dimensions (x, y, z) are given as multiples of depth h. y is the vertical coordinate.

Re_τ	**Re_b (approx)**	**Wall BC**	**Streamwise BC**	**Mesh**	**Comments**
150	2300	Resolved	Periodic	2π×1×π (64×40×64) 4π×1×2π (128×40×128)	Comparison with DNS
			SEM_Saturne	10π×1×2π (300×40×128)	
			SEM_Jarrin	10π×1×2π (300×40×128) 20π×1×2π (600×40×128)	
			DFSEM	10π×1×2π (300×40×128)	
1020	20000	Resolved	Periodic	2π×1×π (256×64×256) 2π×1×π (256×96×256)	Comparison with channel DNS
		Wall functions	Periodic	2π×1×π (96×32×96) 2π×1×π (128×40×128)	
9300	250000	Wall functions	Periodic	2π×1×π (256×64×256) 2π×1×π (256×96×256) 2π×1×π (256×128×256)	Nominal laboratory scale
			SEM_Jarrin	2π×1×π (256×128×256)	
			SEM_Jarrin (constant $L_{\alpha\alpha}$)	2π×1×π (256×128×256)	

To put these Reynolds numbers in perspective, the full-scale Re_b for the EMEC site would be about 30×10^6, corresponding to Re_τ = 630000.

3.4 Results For Fully-Developed Flow

3.4.1 Mean Velocity and Reynolds Stresses In Fully-Developed (Periodic) Flow

Figures 3.1 – 3.4 show the mean velocity, Reynolds shear stress and normal stresses for the following cases:

- Re_τ = 150 (fully-resolved wall treatment)
- Re_τ = 1020 (fully-resolved wall treatment)
- Re_τ = 1020 (wall functions)
- Re_τ = 9300 (wall functions)

Figure 3.1 confirms that grid resolution was sufficient for a wall-resolved LES simulation at Re = 150. Note that our upper boundary condition (stress-free rigid lid) is not precisely that of the DNS conditions (half of a wall-to-wall channel flow); in particular, $\overline{v^2}$ is zero at $y = h$ in the LES results but not in the DNS, with secondary effects on the other components. Also demonstrated by the figure is the insensitivity of results to the size of the free-surface cell.

Figure 3.2 shows the same quantities at the higher Reynolds number, Re_τ = 1020, again in comparison with DNS. There is some sensitivity to grid resolution in the spanwise direction and the difference in upper boundary condition between DNS and LES is slightly more marked (although only really significant in the $\overline{v^2}$ component).

Figure 3.3 differs from Figure 3.2 in that a wall-function treatment was used (resulting in minor aberrations in shear stress at first and second cells from the wall when plotted in wall units). The most significant conclusion from these results is that the Reichardt wall profile (which provides a smooth transition from linear sublayer to log layer) is much less sensitive to the size of the near-wall cell. Above $y^+ = 50$ both wall-function treatments provide mean-velocity and Reynolds stresses in good agreement with DNS, an optimistic result for the higher-Reynolds-number calculations envisaged for a tidal turbine.

Figure 3.4 shows results with wall functions for the highest Reynolds number tested, Re_τ = 9300. A higher sensitivity to grid resolution in the vertical direction is in evidence here. Note again the influence of the free-surface boundary condition, which is now becoming more marked in the streamwise and spanwise normal stresses, in addition to the vertical component more directly affected by the rigid-lid approximation.

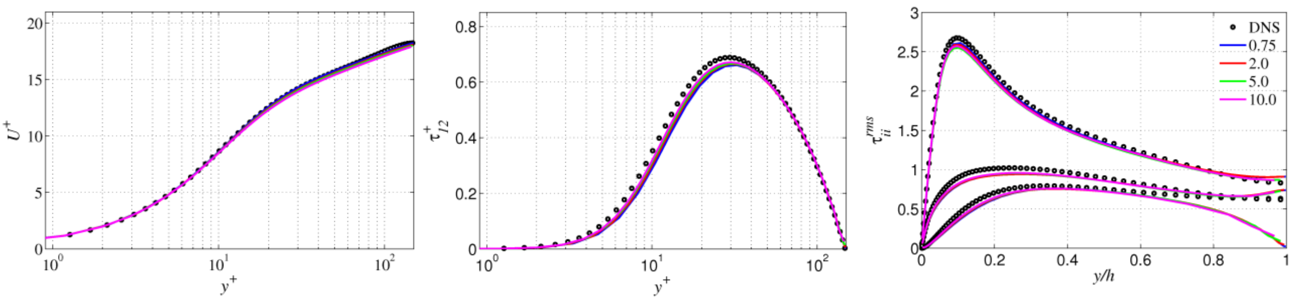

(a) (b) (c)

Figure 3.1: fully-developed flow at Re_τ =150; (a) mean velocity; (b) shear stress; (c) rms normal fluctuations (from top to bottom: $\sqrt{u'^2}$, $\sqrt{w'^2}$, $\sqrt{v'^2}$); cases are the free-surface cell size.

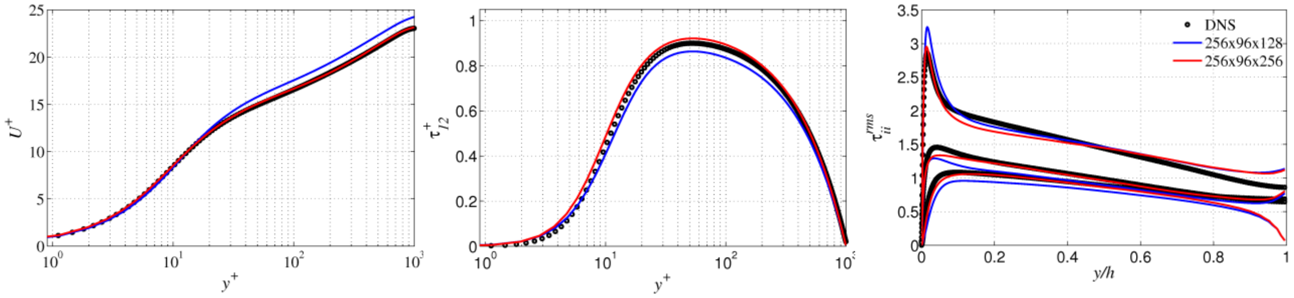

(a) (b) (c)

Figure 3.2: fully-developed flow at Re$_\tau$ =1020; wall-resolved; (a) mean velocity; (b) shear stress; (c) rms normal fluctuations (from top to bottom: $\sqrt{u'^2}$, $\sqrt{w'^2}$, $\sqrt{v'^2}$).

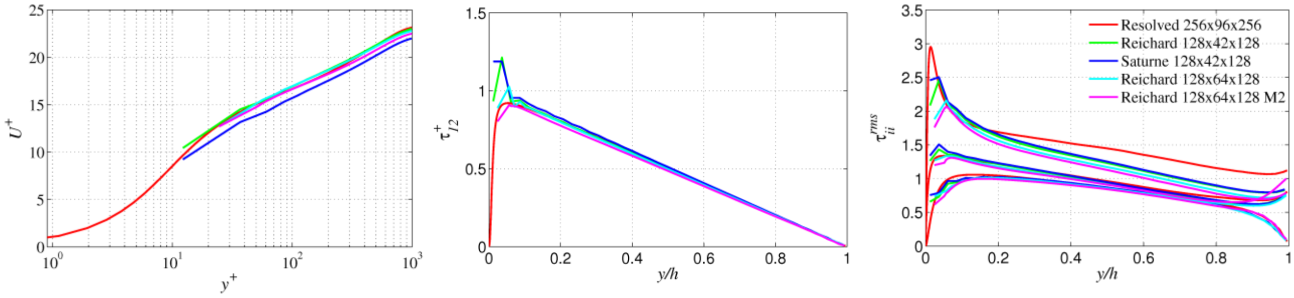

(a) (b) (c)

Figure 3.3: fully-developed flow at Re$_\tau$ = 1020 with wall functions; (a) mean velocity; (b) shear stress; (c) rms normal fluctuations (from top to bottom: $\sqrt{u'^2}$, $\sqrt{w'^2}$, $\sqrt{v'^2}$).

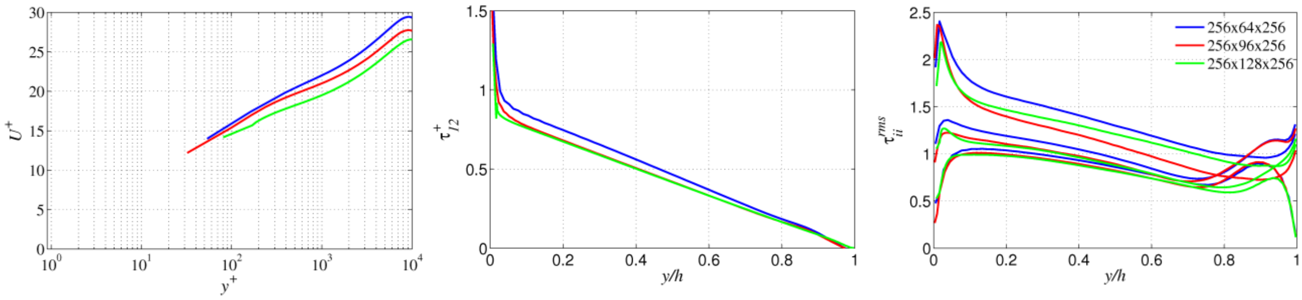

(a) (b) (c)

Figure 3.4: fully-developed flow at Re$_\tau$ = 9300; (a) mean velocity; (b) shear stress; (c) rms normal fluctuations (from top to bottom: $\sqrt{u'^2}$, $\sqrt{w'^2}$, $\sqrt{v'^2}$).

3.4.2 Length Scales In Fully-Developed (Periodic) Flow

Figures 3.5 and 3.6 show the possible choices of length scales at $Re_\tau = 150$:

- coloured lines showing (at two grid resolutions) integral length scales L_{11}, L_{22}, L_{33} deduced from two-point correlations;
- solid black lines showing the anisotropic length scales L_{11}, L_{22}, L_{33} based on the corresponding normal stresses (equation 3.2);
- dashed black line showing the isotropic length scale L_k based on turbulent kinetic energy (equation 3.1).

The different length scales are naturally different quantities! There is no presumption that they should be equal, but we seek to both characterise their behaviour and establish whether the simpler length scales based on Reynolds stresses might exhibit similar behaviour to the correlation length scales more appropriate for synthetic-eddy modelling.

Note that Figure 3.5 shows integral length scales based on streamwise correlations, whilst Figure 3.6 shows the corresponding quantities based on spanwise correlations. The length scales based on normal stresses and turbulent kinetic energy are the same in both Figures.

With the exception of the streamwise L_{11} components (coloured lines on the first graph in Figure 5) the integral length scales are essentially grid-independent. The reason for the difference in this particular case is that the correlation in the streamwise direction does not decay rapidly in this direction. In general, no length scales based on the normal stresses accurately reflect the behaviour of the integral length scales: in particular, they do not produce the large structures/extended correlation near the wall.

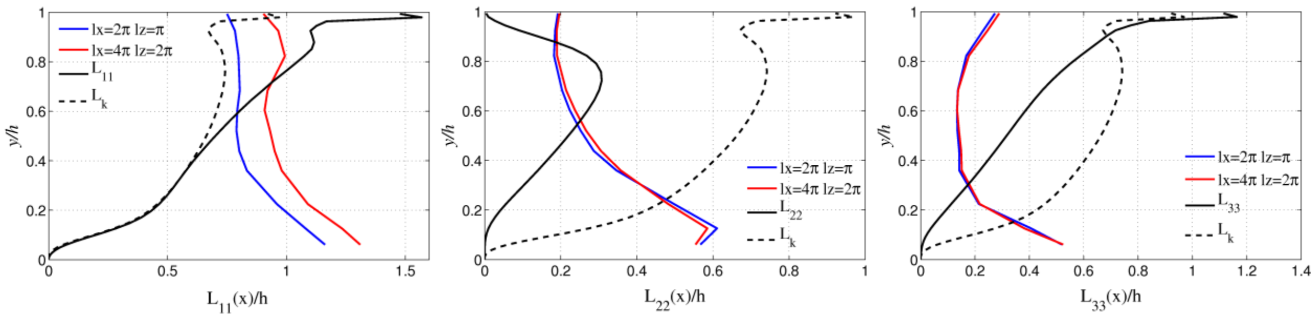

Figure 3.5: fully-developed flow at $Re_\tau = 150$; streamwise integral length scales, compared with those deduced from normal stresses or turbulent kinetic energy.

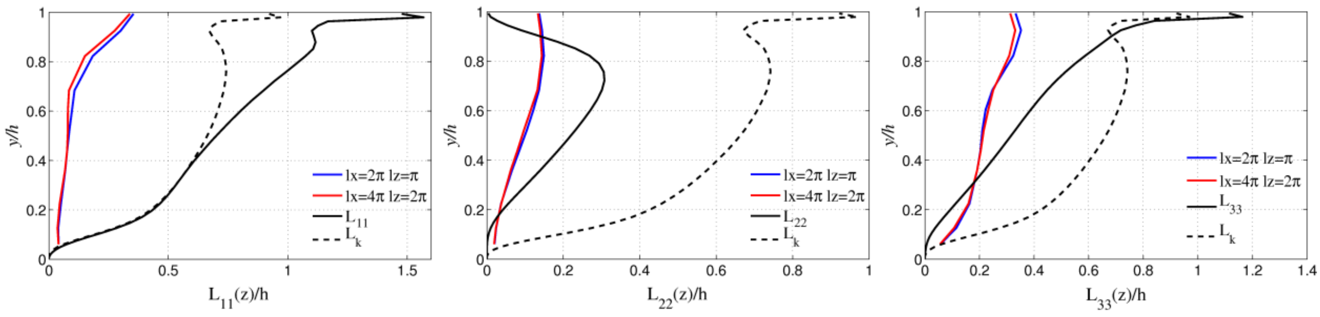

Figure 3.6: fully-developed flow at $Re_\tau = 150$; spanwise integral length scales, compared with those deduced from normal stresses or turbulent kinetic energy.

Figures 3.7 and 3.8 show integral length scales at $Re_\tau = 1020$, comparing wall-function and wall-resolved computations. There are clearly wiggles in the wall-function profiles, probably due to the substantially-coarser resolution in the vertical. However, filtering this, there is good agreement between the two approaches with the single exception of the streamwise L_{11} integral length scale. This may be due to near-wall structures not being resolved by the wall-function approach.

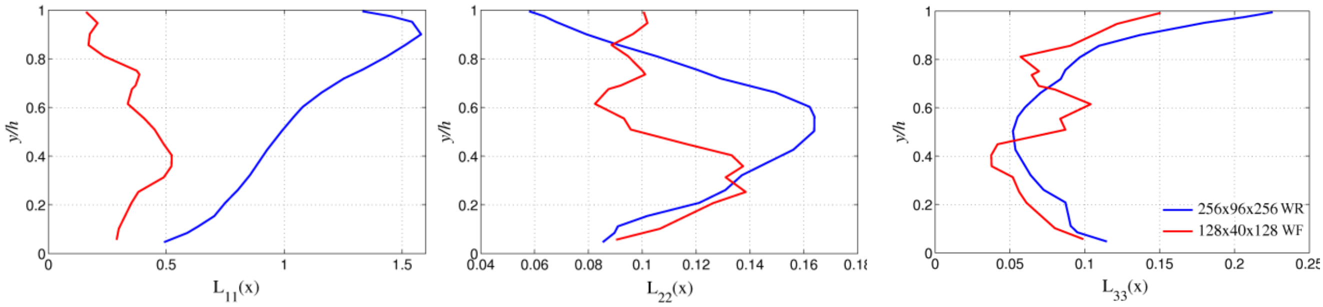

Figure 3.7: fully-developed flow at $Re_\tau = 1020$; streamwise integral length scales.

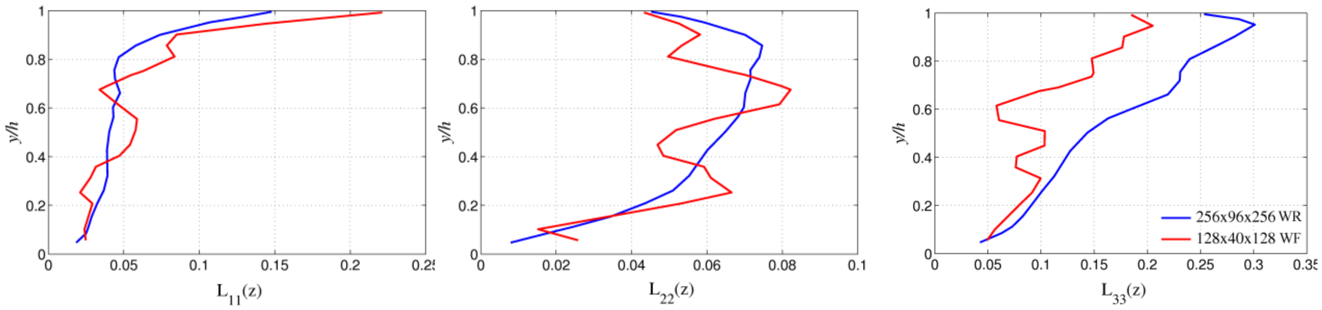

Figure 3.8: fully-developed flow at $Re_\tau = 1020$; spanwise integral length scales.

Figures 3.9 and 3.10 show integral length scales at $Re_\tau = 9300$, computed using wall functions. In this case there is broader agreement in the L_{11} scale with the wall-resolved computation at the lower Reynolds number (compare L_{11} in Figure 3.9 with that in Figure 3.7). Both show a length scale growing approximately linearly with distance from the wall boundary, up to a maximum of 1.2 – 1.5 times depth at approximately 80% of channel depth.

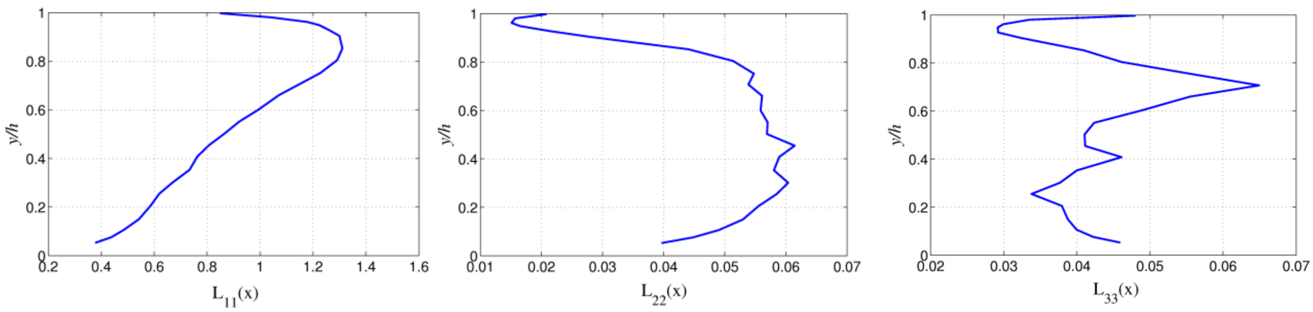

Figure 3.9: fully-developed flow at $Re_\tau = 9300$; streamwise integral length scales.

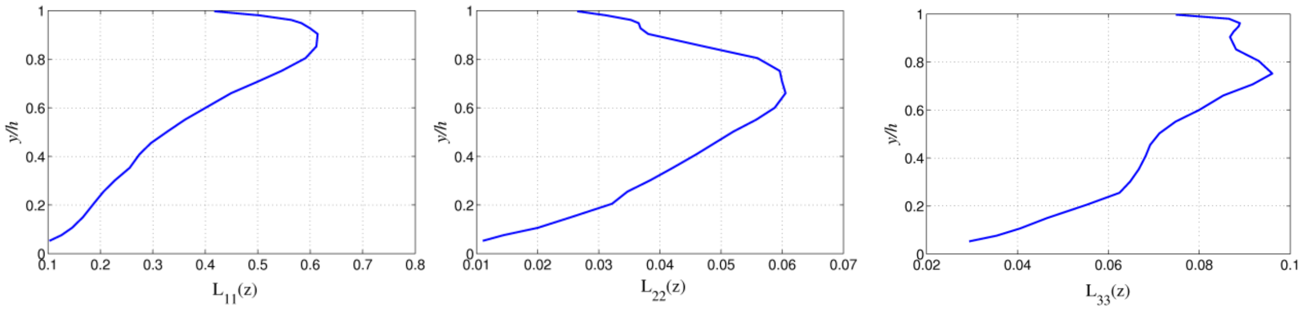

Figure 3.10: fully-developed flow at Re_τ = 9300; spanwise integral length scales.

3.5 Results With Synthetic-Eddy Methods For Developing Flow

A key finding was that the different variants of SEM model actually gave very similar results for mean velocity and Reynolds stress and their rate of development. Thus, the major interest lies in the difference between SEM and DFSEM.

Two Reynolds numbers were examined: $Re_\tau = 150$ and $Re_\tau = 9300$, the former using wall-resolved lower-boundary treatment and the latter wall functions. In each case the mean velocity at inlet was that determined from the periodic solutions, whilst turbulent fluctuations were supplied synthetically.

<u>$Re_\tau = 150$</u>

Figures 3.11 – 3.15 show the development of mean velocity, the three normal stresses and the Reynolds shear stress with distance at $Re_\tau = 150$. All synthetic-eddy methods tested – SEM_Saturne (with three length scales), SEM_Jarrin (with seven length scales) and DFSEM – are shown. The graphs show profiles at streamwise locations x/h = 0, 10, 20, 29 downstream of the inlet plane. Note that the DFSEM exhibits a considerable departure from the intended Reynolds-stress profiles at inlet (which may be a coding error – still to be investigated – or a reflection of the model's inability to represent accurately all states of anisotropy). However, it is also clear that the DFSEM, as was hoped, leads to a considerably shorter development length than the original SEM; indeed the fully-developed Reynolds-stress profile is not recovered by the latter model within the computational domain.

Figures 3.16 – 3.20 present the same information in more visual, if less quantitative, form. As the two SEM approaches gave very similar results only the SEM_Jarrin results are shown.

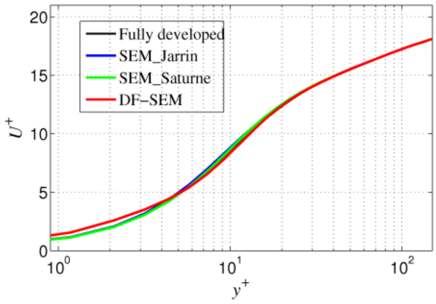

(a)

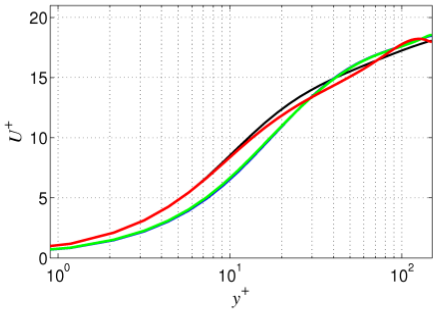

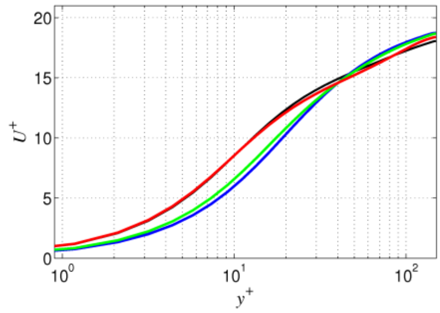

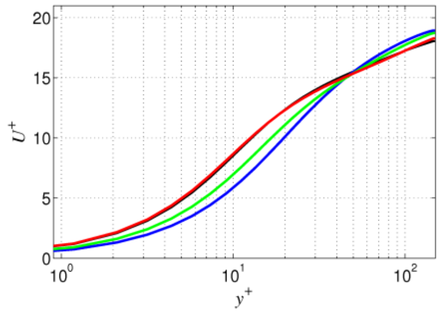

(b) (c) (d)

Figure 3.11: development of mean-velocity with synthetic turbulence; Re_τ = 150; (a) *x*/*h* = 0; (b) *x*/*h* = 10; (c) *x*/*h* = 20; (d) *x*/*h* = 29.

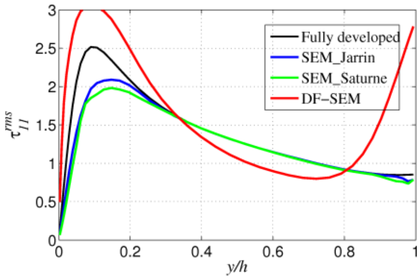

(a)

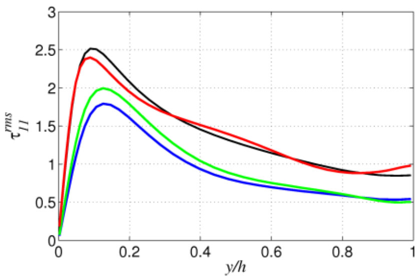

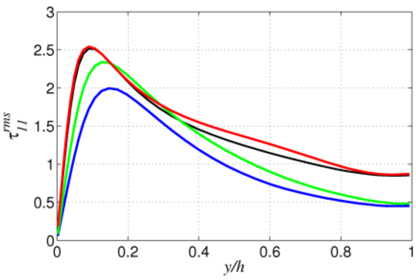

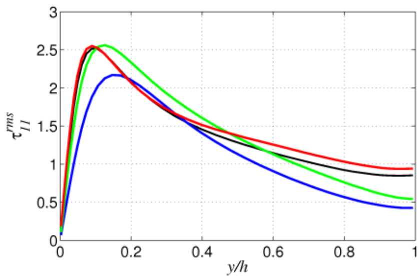

(b) (c) (d)

Figure 3.12: development of $\overline{u^2}$ with synthetic turbulence; Re_τ = 150; (a) *x*/*h* = 0; (b) *x*/*h* = 10; (c) *x*/*h* = 20; (d) *x*/*h* = 29.

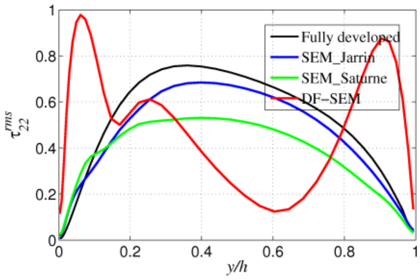

(a)

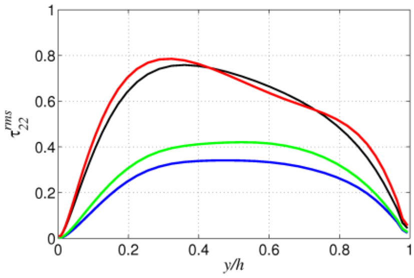

(b)

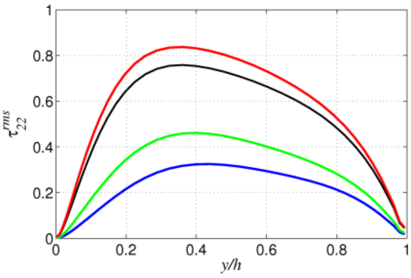

(c)

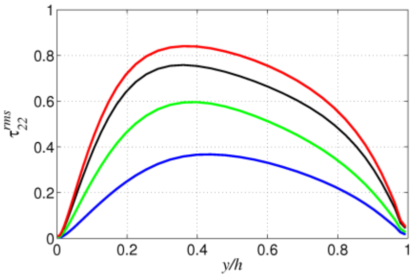

(d)

Figure 3.13: development of $\overline{v^2}$ with synthetic turbulence; Re$_\tau$ = 150;
(a) *x*/*h* = 0; (b) *x*/*h* = 10; (c) *x*/*h* = 20; (d) *x*/*h* = 29.

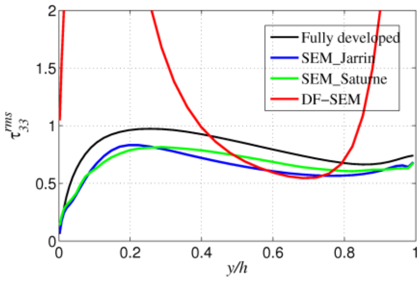

(a)

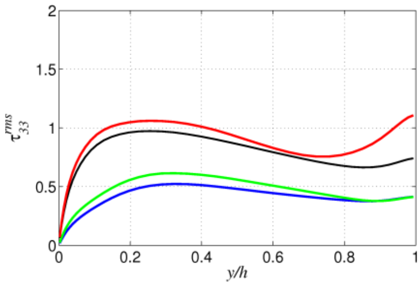

(b)

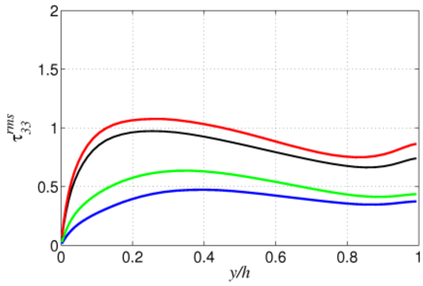

(c)

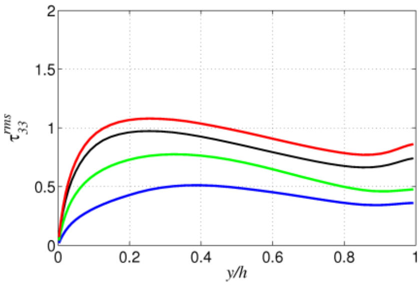

(d)

Figure 3.14: development of $\overline{w^2}$ with synthetic turbulence; Re$_\tau$ = 150;
(a) *x*/*h* = 0; (b) *x*/*h* = 10; (c) *x*/*h* = 20; (d) *x*/*h* = 29.

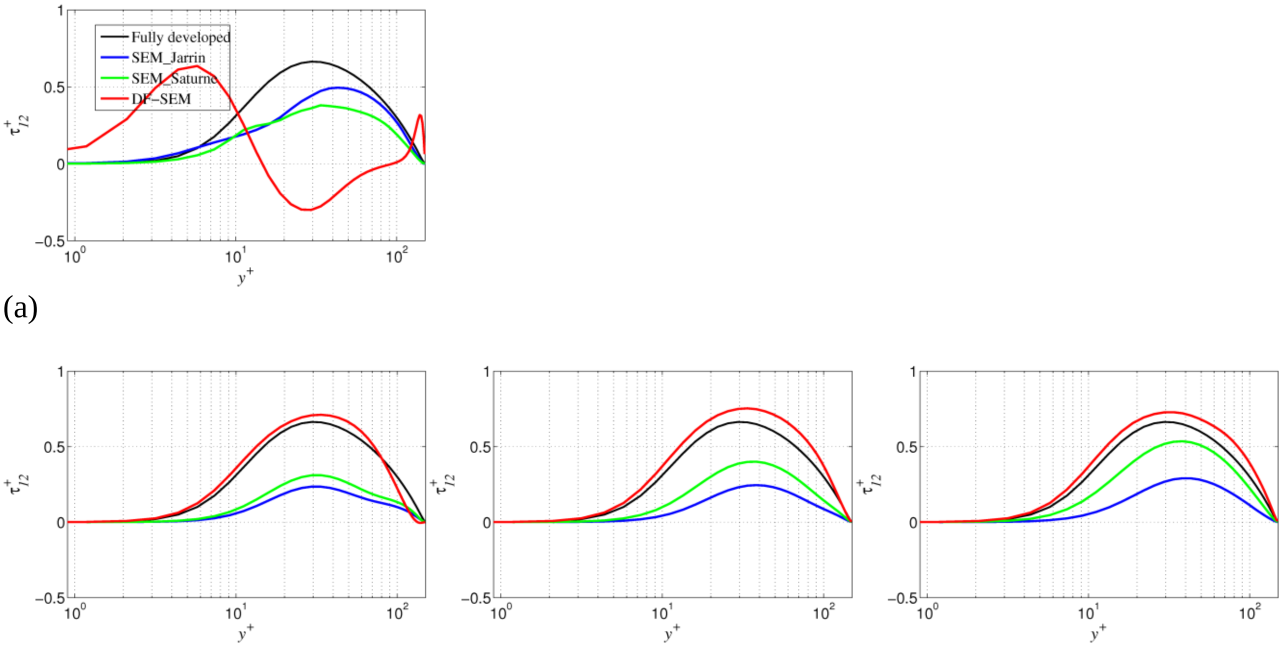

(a)

(b) (c) (d)

Figure 3.15: development of $\overline{-uv}$ with synthetic turbulence; Re$_\tau$ = 150;
(a) *x*/*h* = 0; (b) *x*/*h* = 10; (c) *x*/*h* = 20; (d) *x*/*h* = 29.

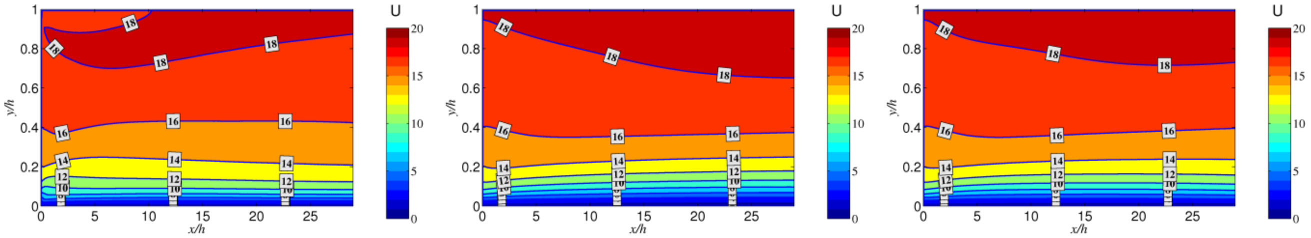

(a) (b) (c)

Figure 3.16: development of mean velocity with synthetic turbulence; $Re_\tau = 150$; (a) DFSEM; (b) SEM_Jarrin; (c) SEM_Saturne

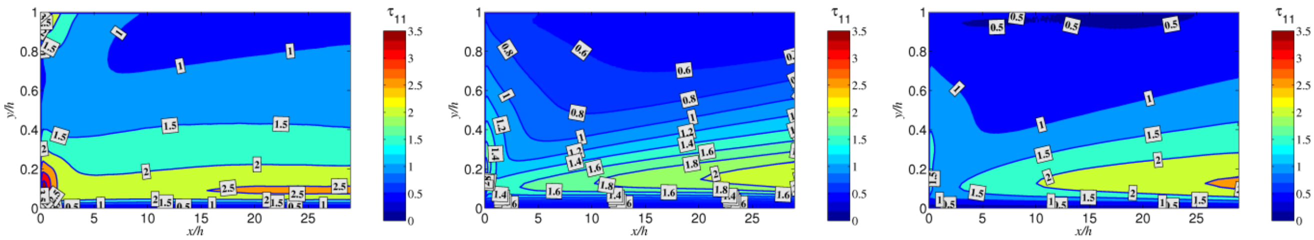

(a) (b) (c)

Figure 3.17: development of $\overline{u^2}$ with synthetic turbulence; $Re_\tau = 150$; (a) DFSEM; (b) SEM_Jarrin; (c) SEM_Saturne

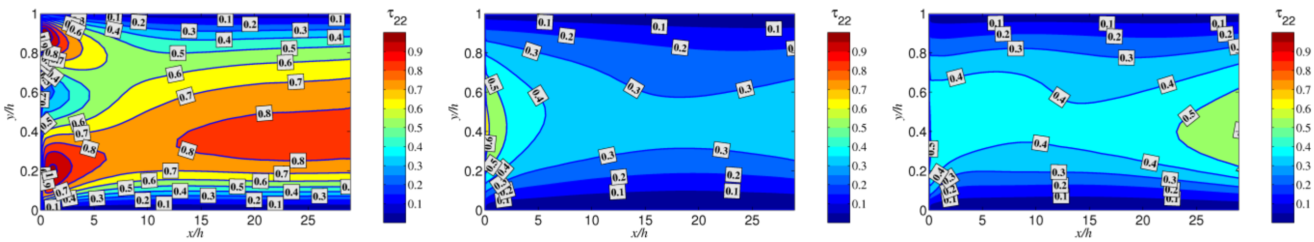

(a) (b) (c)

Figure 3.18: development of $\overline{v^2}$ with synthetic turbulence; $Re_\tau = 150$; (a) DFSEM; (b) SEM_Jarrin; (c) SEM_Saturne

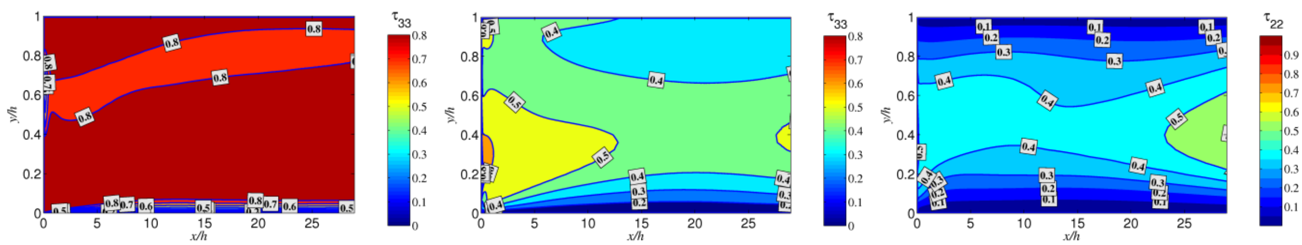

(a) (b) (c)

Figure 3.19 development of $\overline{w^2}$ with synthetic turbulence; $Re_\tau = 150$; (a) DFSEM; (b) SEM_Jarrin; (c) SEM_Saturne

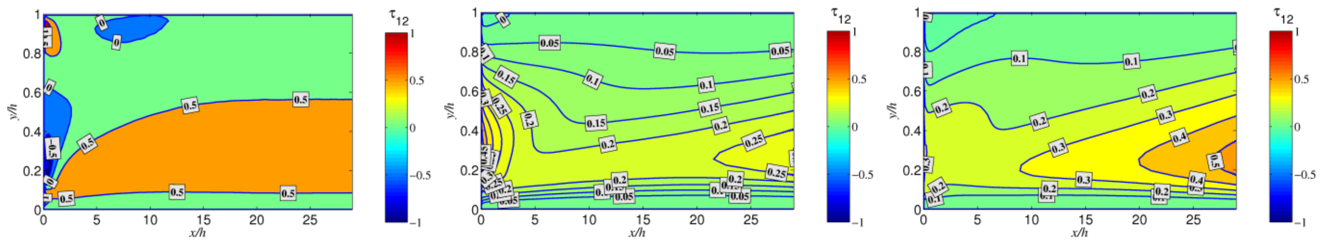

(a) (b) (c)

Figure 3.20 development of $-\overline{uv}$ with synthetic turbulence; Re_τ = 150; (a) DFSEM; (b) SEM_Jarrin; (c) SEM_Saturne

Re$_\tau$ = 9300

It was intended to carry out similar calculations at this higher Reynolds number, but at present stable DFSEM results have not been obtained for this case. (The inaccurate representation of the intended Reynolds stresses at the inlet plane suggests a possible coding error, but further investigation will be needed to determine this.) The results for this Reynolds number are only for the SEM_Jarrin variant; in this instance we have compared them with a SEM calculations using a single length scale (based on the streamwise integral length at mid-depth). The latter would be considerably easier to determine from experimental data.

Figures 3.21 – 3.25 show line graphs of the streamwise evolution of mean velocity, normal stresses and shear stress, whilst Figures 3.26 – 3.30 show two-dimensional contour plots of the same quantities.

It is observed that, at this high Reynolds number, the profiles evolve very slowly in the streamwise direction, the channel maxima of normal stresses being obtained by about 4 channel depths from the inlet plane.

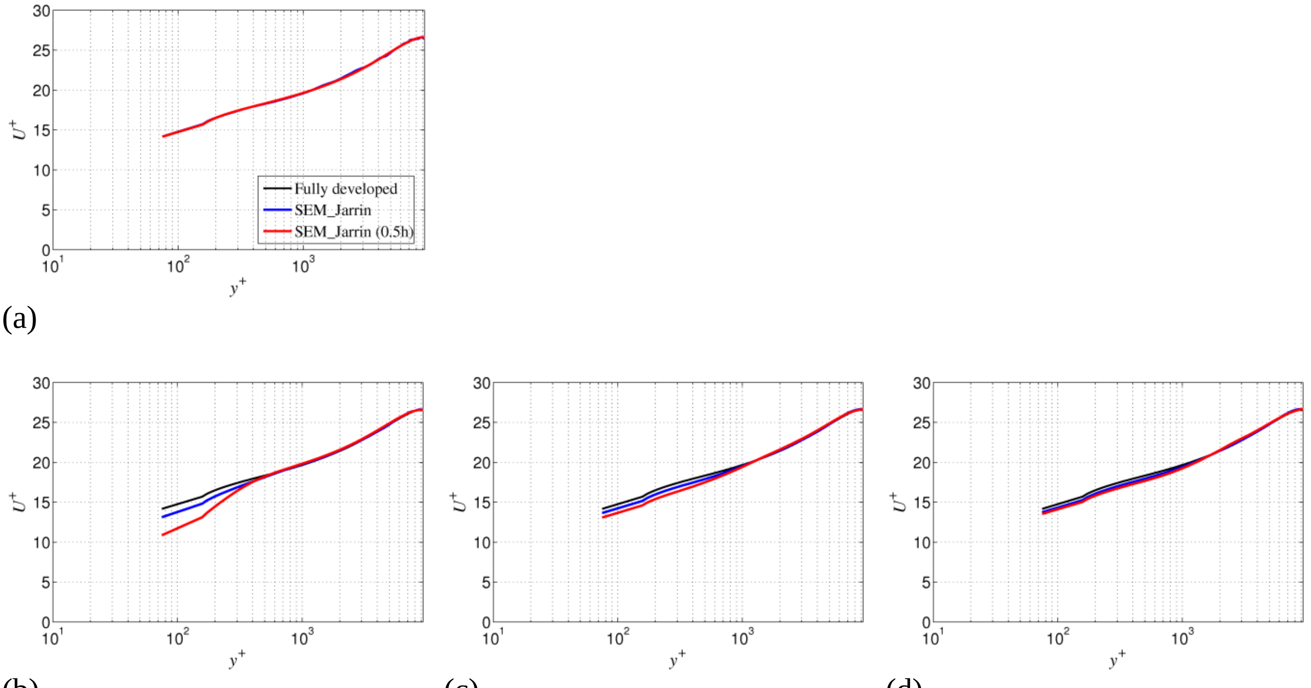

(a)

(b) (c) (d)

Figure 3.21: development of mean-velocity with synthetic turbulence (SEM_Jarrin); Re$_\tau$ = 9300; (a) *x*/*h* = 0; (b) *x*/*h* = 2; (c) *x*/*h* = 4; (d) *x*/*h* = 6.

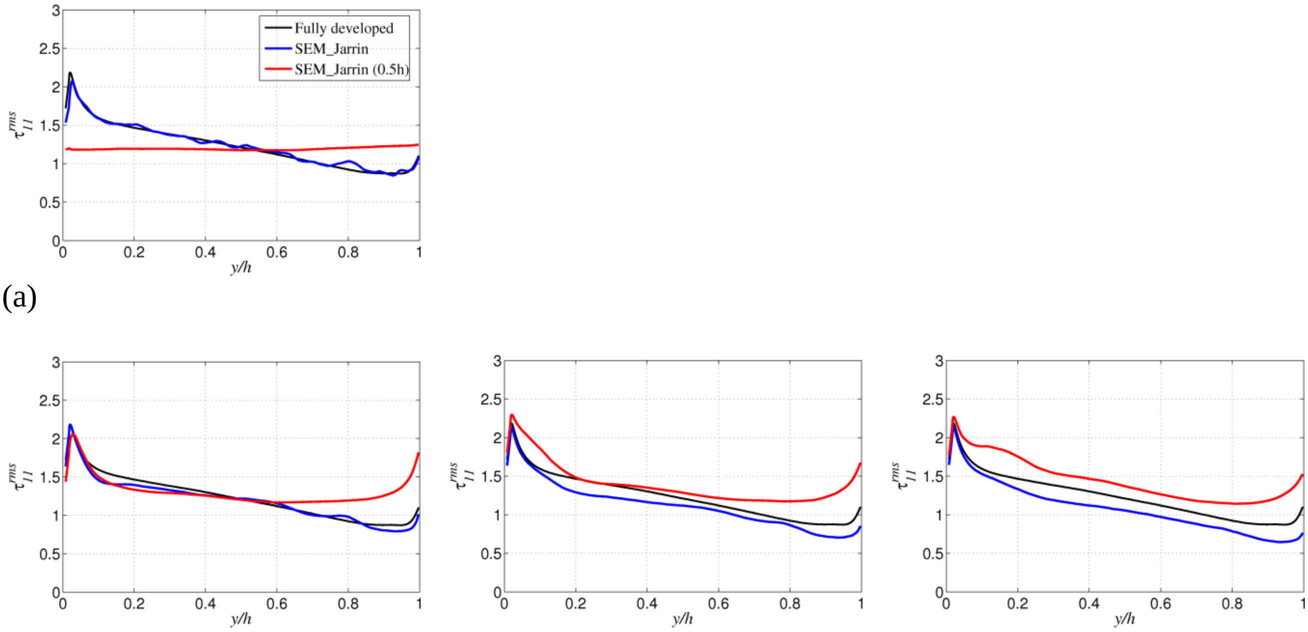

(a)

(b) (c) (d)

Figure 3.22: development of $\overline{u^2}$ with synthetic turbulence (SEM_Jarrin); Re$_\tau$ = 9300; (a) *x*/*h* = 0; (b) *x*/*h* = 2; (c) *x*/*h* = 4; (d) *x*/*h* = 6.

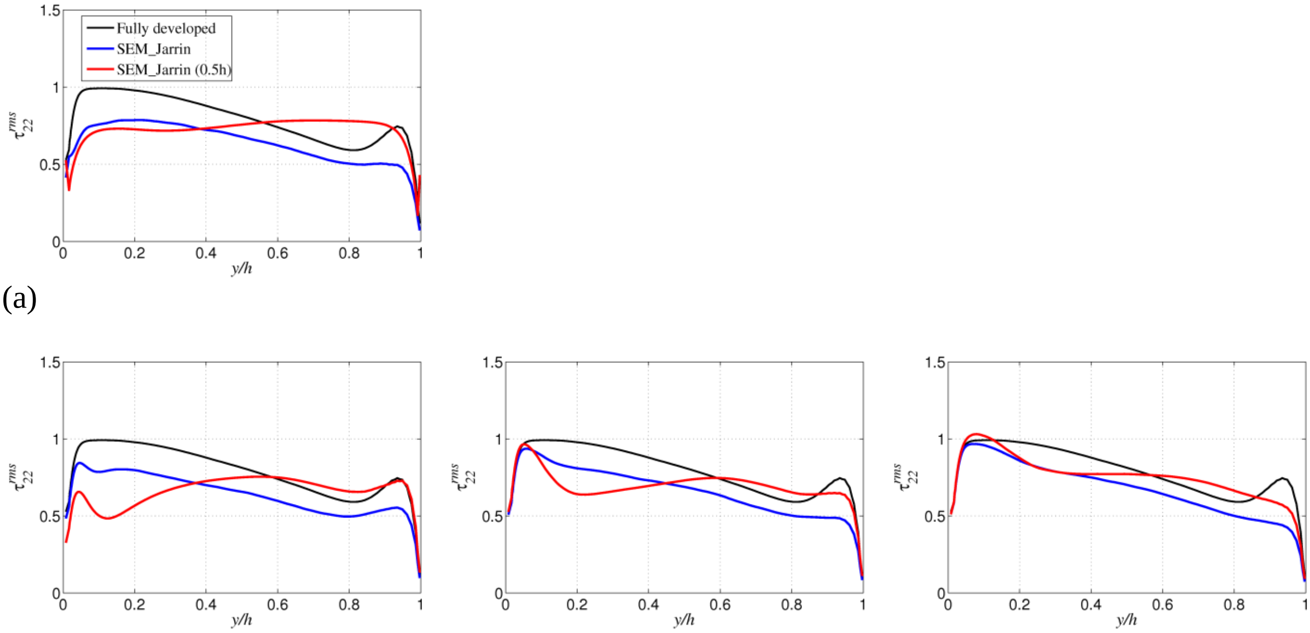

(a)

(b) (c) (d)

Figure 3.23: development of $\overline{v^2}$ with synthetic turbulence (SEM_Jarrin); Re$_\tau$ = 9300; (a) *x*/*h* = 0; (b) *x*/*h* = 2; (c) *x*/*h* = 4; (d) *x*/*h* = 6.

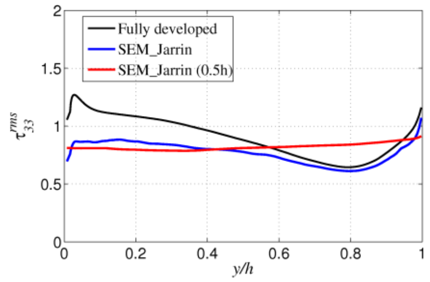

(a)

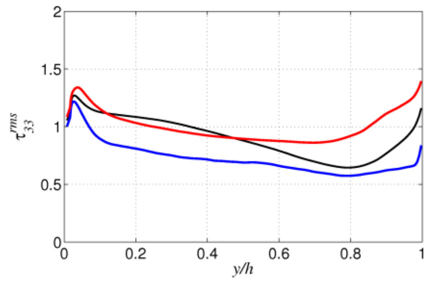

(b)

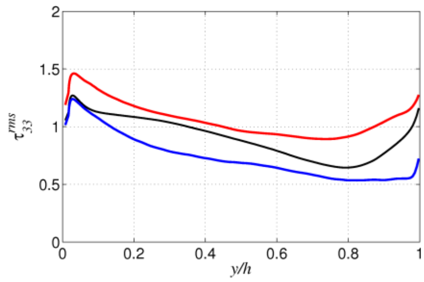

(c)

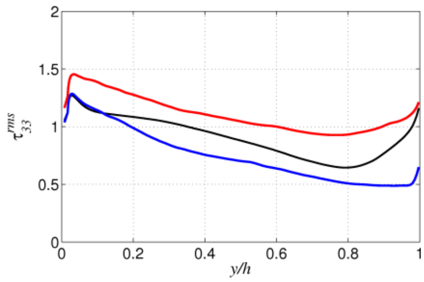

(d)

Figure 3.24: development of $\overline{w^2}$ with synthetic turbulence (SEM_Jarrin); Re_τ = 9300; (a) *x*/*h* = 0; (b) *x*/*h* = 2; (c) *x*/*h* = 4; (d) *x*/*h* = 6.

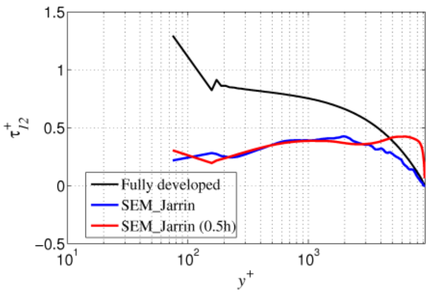

(a)

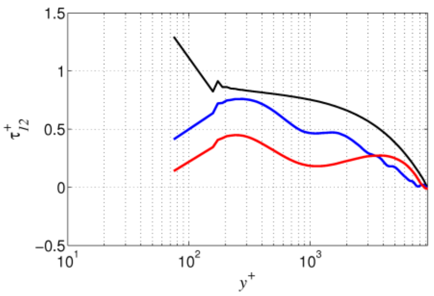

(b)

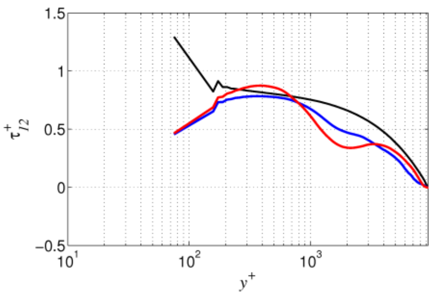

(c)

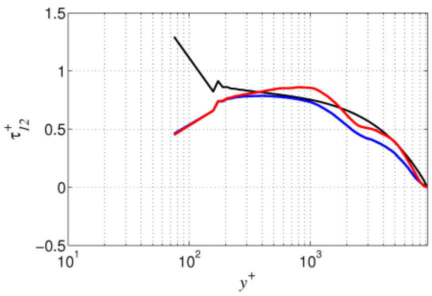

(d)

Figure 3.25: development of $-\overline{uv}$ with synthetic turbulence (SEM_Jarrin); Re_τ = 9300; (a) *x*/*h* = 0; (b) *x*/*h* = 2; (c) *x*/*h* = 4; (d) *x*/*h* = 6.

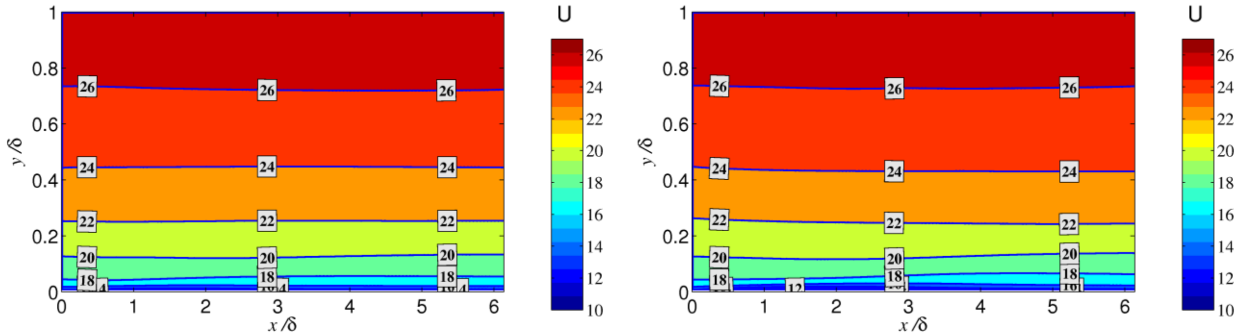

Figure 3.26: development of mean velocity with synthetic turbulence; Re_τ = 9300; (a) 7 length scales; (b) single length scale based on mid-depth.

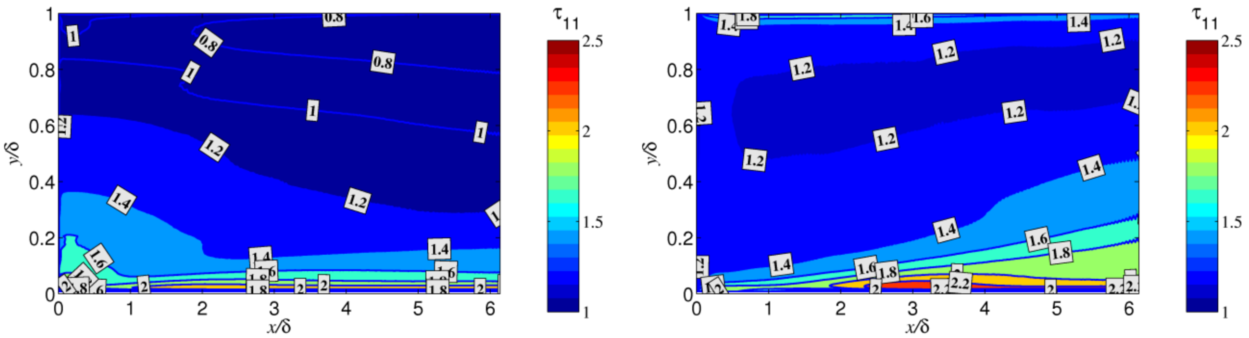

Figure 3.27: development of $\overline{u^2}$ with synthetic turbulence; Re_τ = 9300; (a) 7 length scales; (b) single length scale based on mid-depth.

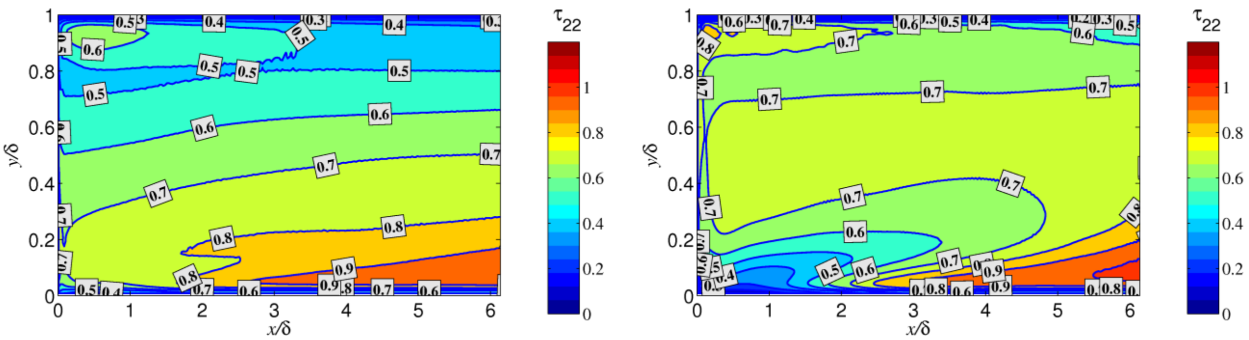

Figure 3.28: development of $\overline{v^2}$ with synthetic turbulence; Re_τ = 9300; (a) 7 length scales; (b) single length scale based on mid-depth.

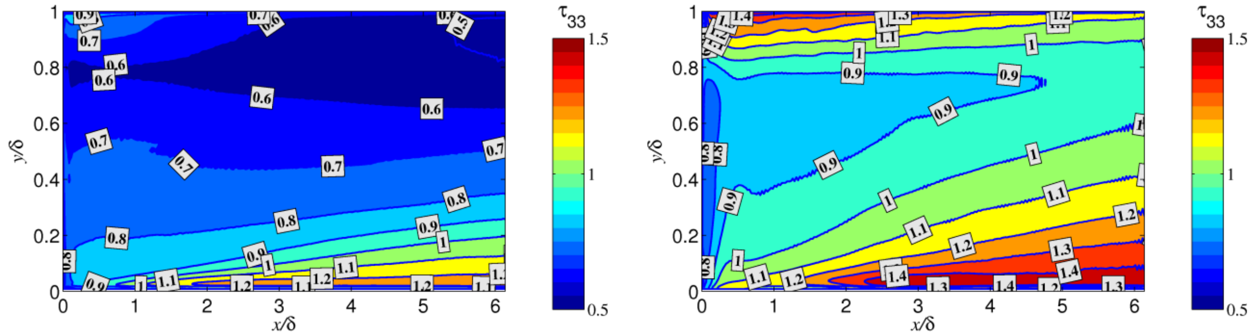

Figure 3.29: development of $\overline{w^2}$ with synthetic turbulence; Re_τ = 9300; (a) 7 length scales; (b) single length scale based on mid-depth.

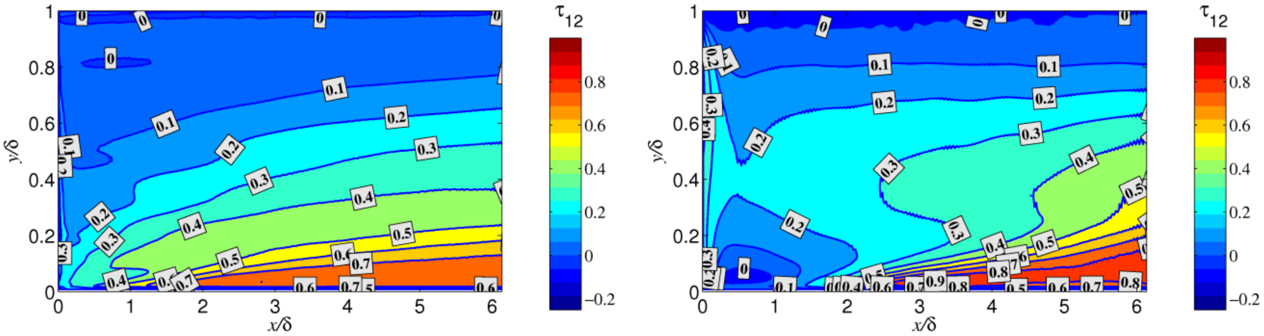

Figure 3.30: development of $-\overline{uv}$ with synthetic turbulence; Re_τ = 9300; (a) 7 length scales; (b) single length scale based on mid-depth.

4. OUTLINE OF FUTURE WORK

The main aim of the MD1.1-MD1.5 package is to evaluate the accuracy with which CFD – in particular, LES – predicts the time-varying loads on a full-scale tidal-stream turbine subject to flow representative of measurements from the EMEC site. To complete these aims (in the out-of-sequence report MD1.4) it is necessary to:

(1) develop a suitable mesh for (i) the rotating turbine region; (ii) the channel;
(2) specify appropriate inflow conditions for mean velocity and turbulence;
(3) specify mechanical aspects during operation.

These are examined individually below.

4.1 Computational Mesh

For the RANS calculation the rotating (turbine) block currently has 2.8 million cells, whilst the outer domain has 5.6 million cells.

For the rotating part of the mesh it is required to obtain a mesh with sufficient near-wall cells to resolve the boundary layer on the wetted surface of the turbine. In MD1.2 the LES simulations of the loading of a generic turbine were performed with $y^+ < 5$ across the blade surface. A mesh of the TGL 1 MW geometry has been built and employed for RANS simulations. Refinement of this mesh to meet the same y^+ criteria is expected to produce an LES mesh for the *rotor region* with approximately 10 million cells.

For the stationary outer part of the mesh, sufficient resolution is required to model propagation of turbulence with streamwise length scale of the order of the channel depth (see Figure 3.9). The Reynolds number of the EMEC flow is considerably higher than the simulations conducted to date (roughly $Re_b = 30\times10^6$, corresponding to $Re_\tau = 630000$). A fully-resolved LES simulation at this Reynolds number would be prohibitively expensive. Since the focus of the simulations is on turbine loading, a coarser mesh will be employed in the channel region where possible to minimize computational cost. The Re_τ = 9300 simulations provide information for defining the structure of a suitable mesh.

- In the vertical, a mesh with near-wall y^+ of 240 provides a reasonable prediction of the depth profile of the mean flow and turbulence length-scales when a Reichardt wall function is applied at the bed.
- In the spanwise direction, RANS simulations of the TGL rotor were conducted with a channel width of four diameters, approximately $1.3\pi h$; the LES channel-flow simulations demonstrated that a channel width of πh was sufficient to resolve the spanwise length scales.
- In the streamwise direction we consider separately the upstream and downstream regions. To establish the loading on the turbine it is important that turbulence structures in the approach flow be resolved. For the wake region a similar approach will be employed to that of earlier LES studies (MD1.2) with a coarser mesh used downstream of the rotor plane. The selection of an appropriate upstream distance is related to the choice of inflow turbulence model (see below).

Based on these considerations it is expected that the channel mesh will comprise approximately 18 million cells.

The combined requirements of resolving the turbine boundary layer and approach-flow turbulence structures therefore suggest a total mesh size of about 28 million cells.

4.2 Specification of Turbulence and Velocity Profile

In this study we have considered three synthetic turbulence models for defining onset turbulence with coherent structure. These approaches differ in terms of the number (and type) of length scales required to specify the model and in terms of the distance required for turbulence statistics to develop downstream of the inflow. The performance of each has been evaluated by comparison to the profile of mean velocity and turbulence statistics for a fully-developed channel flow. The main findings related to the MD1.4 simulations are the following.

- The development distance reduces with increasing Reynolds number ($Re_\tau = 150$ to 9300). This is expected to reduce further as Re_τ is increased to 630000, although the minimum development distance is expected to correspond to small multiples of the streamwise length-scale. The latter is roughly equal to the water depth, so that a distance of 2 to 3 depths upstream is expected to be suitable.

- There is some evidence from the lower-Re calculations that the divergence-free synthetic-eddy model requires a shorter distance to develop the mean velocity depth profile and Reynolds stresses than either of the standard SEM. However, the EMEC flow differs considerably from a fully- developed flow in a periodic channel since the flow is dependent on the upstream bathymetry of the site (and on the stage in the tidal cycle). For this case the near-bed Reynolds stresses developed by DFSEM are expected to lead to diffusion of any defined, non-developed, mean-velocity profile within a short distance of the inflow. For the EMEC flows, one of the available SEM is therefore more suitable.

- The SEM defined by 3 stress-based length scales requires a shorter development length at low Reynolds number ($Re_\tau = 150$) than the SEM defined by six integral and one stress-dependent length scales. However, the two approaches are comparable at $Re_\tau = 9300$. At this Reynolds number the fully-developed mean velocity is recovered within approximately 6h of inflow, but the Reynolds stresses take longer to recover. Use of a single length scale over the full depth of the channel (Figures 3.21 – 3.25) is not as effective as full-depth profiles; however, if a length scale at a single depth was provided it would be possible to scale our existing simulation results to give the full channel profile.

To completely define these models the following data is required from the field measurements:
(a) complete depth profile of mean streamwise velocity;
(b) complete depth profile of normal Reynolds stresses and length scales.

If (b) were not available then the magnitude of stresses and length scales at a single depth could be employed, with the full depth profiles determined from our channel-flow simulations.

4.3 Specification of Mechanical Aspects

The TGL turbine controller continuously adjusts pitch to ensure that rated speed and power are not exceeded. It is not feasible to model continuous pitch control in the CFD model and so each CFD simulation will represent an interval of constant pitch. Each pitch angle will require a different rotor mesh. Each simulation is expected to be approximately 1-minute duration real time. This constant pitch requirement has been discussed by the University of Manchester and TGL and is incorporated in Test Request Note (TRN) 317. GHTidalBladed simulations have been run (by TGL) to confirm that the turbine controller can be set such that blade pitch can safely be maintained at a constant value for suitable intervals during the mean speeds of 1.8 m s^{-1} and 2.8 m s^{-1} that are of interest for MD1.4 simulations. Further discussions on the exact values to use will follow turbine commissioning.

REFERENCES

Abe, H., Kawamura, H., and Matsuo, Y. (2004). Surface heat-flux fluctuations in a turbulent channel flow up to Re_τ = 1020 with Pr = 0.025 and 0.71. International Journal of Heat and Fluid Flow 25(3), 404 – 419.

Bahaj, A. S., Batten, W. M. J., Molland, A. F., and Chaplin, J. R. (2005). Experimental investigation into the effect of rotor blade sweep on the performance of marine current turbines. Proceedings of the Institution of Mechanical Engineers, Part A: Journal of Power and Energy, 215(5), 611-622.

Gant, S. and Stallard, T. (2008). Modelling a tidal turbine in unsteady flow. In: Proceedings of the Eighteenth International Offshore and Polar Engineering Conference, number 2007, 473-479.

Jarrin, N., Benhamadouche, S., Laurence, D. and Prosser, R. (2006). A synthetic-eddy method for generating inflow conditions for large-eddy simulations. International Journal of Heat and Fluid Flow 27(4), 585 – 593.

Jarrin, N., Prosser, R., Uribe, J., Benhamadouche, S. and Laurence, D. (2009). Reconstruction of turbulent fluctuations for hybrid RANS/LES simulations using a synthetic-eddy method. International Journal of Heat and Fluid Flow 30(3), 435 – 442.

McNaughton, J., Rolfo, S., Apsley, D., Afgan, I., Stansby, P., and Stallard, T. (2012). CFD prediction of turbulent flow on an experimental tidal stream turbine using RANS modelling. In: Proceedings of the 1st Asian Wave and Tidal Energy Conference, Jeju Island, South Korea.

Poletto, R., Revell, A., Craft, T. and Jarrin, N. (2011). Divergence-free synthetic-eddy method for embedded LES inflow boundary conditions. In: Seventh International Symposium On Turbulence and Shear Flow Phenomena (TSFP-7), Ottawa.

Pope, S. B. (2000). Turbulent Flows. Cambridge University Press

Reichardt, H. (1951). Vollstandige Darstellung der turbulenten Geschwindigkeitsverteilung in glatten Leitungen. Z . angew Math. Mech., 31, 208.